



**DISTRIBUTION STATEMENT A**

Approved for public release;  
Distribution Unlimited

COMPUTER AIDED DETECTION OF  
MICROCALCIFICATIONS USING TEXTURE ANALYSIS

THESIS  
Ronald C. Dauk  
Captain, USAF

AFIT/GEO/ENG/95D-01

19960410 022

DEPARTMENT OF THE AIR FORCE  
AIR UNIVERSITY  
**AIR FORCE INSTITUTE OF TECHNOLOGY**

Wright-Patterson Air Force Base, Ohio

DTIC QUALITY INSPECTED 1

AFIT/GEO/ENG/95D-01

COMPUTER AIDED DETECTION OF  
MICROCALCIFICATIONS USING TEXTURE ANALYSIS

THESIS  
Ronald C. Dauk  
Captain, USAF

AFIT/GEO/ENG/95D-01

Approved for public release; Distribution Unlimited

The views expressed in this thesis are those of the author and do not reflect the official policy or position of the Department of Defense or the U. S. Government.

AFIT/GEO/ENG/95D-01

Computer Aided Detection of Microcalcifications Utilizing Texture Analysis

THESIS

Presented to the Faculty of the Graduate School of Engineering  
of the Air Force Institute of Technology

Air University

In Partial Fulfillment of the  
Requirements for the Degree of  
Master of Science in Electrical Engineering

Ronald C. Dauk, B.S. Electrical and Electronics Engineering  
Captain, USAF

December, 1995

Approved for public release; Distribution Unlimited

### *Acknowledgements*

I would like to sincerely thank my advisor, Doctor Steven K. Rogers, for his tremendous support and encouragement. My gratitude also goes to my committee members, Majors Dennis Ruck and Jeff Hoffmeister, and Capt Rick Raines, for their comments and assistance. Major Jeff Hoffmeister deserves a hearty thank you for all his time and effort spent reviewing images for the Computer Aided Breast Cancer detection group. Additionally, I would like to thank the Wright-Patterson AFB Hospital for their cooperation and assistance in developing our mammographic database.

I must also recognize the Breast Cancer Detection Group – Bill, Dru, Amy, Sean, and Dave – for their support and contributions. Dave and Dan, thanks for the loan of the disk space and Sparcs, without you guys this thesis would never of been finished.

Most of all, I would like to thank my family for supporting me over the last year and a half. Willy and Ellen, you were always there to make me laugh and remind me about the important things in life. And last, but definitely not least, Susan, I don't think I could put into words my thanks and gratitude for everything you have done. I could not dream of having a better partner in life. Thank you for everything.

Ronald C. Dauk

## *Table of Contents*

	Page
Acknowledgements . . . . .	ii
List of Figures . . . . .	vi
List of Tables . . . . .	viii
Abstract . . . . .	x
 I. Introduction . . . . .	 1-1
1.1 Breast Cancer Information . . . . .	1-1
1.2 Computer Aided Diagnosis . . . . .	1-2
1.3 Problem Statement . . . . .	1-2
1.4 Scope . . . . .	1-3
1.5 Overview . . . . .	1-4
 II. Background . . . . .	 2-1
2.1 Breast Cancer . . . . .	2-1
2.2 Computer-Aided Diagnosis: Model Based Vision . . . . .	2-3
2.2.1 Focus of Attention . . . . .	2-3
2.2.2 Indexing . . . . .	2-4
2.2.3 Feature Extraction . . . . .	2-4
2.2.4 Prediction . . . . .	2-6
2.2.5 Matching . . . . .	2-6
2.2.6 Search . . . . .	2-6
2.3 Feature Selection . . . . .	2-7
2.4 Summary . . . . .	2-8

	Page
III. Methodology . . . . .	3-1
3.1 Introduction . . . . .	3-1
3.2 Database . . . . .	3-1
3.3 System Overview . . . . .	3-2
3.4 Focus of Attention . . . . .	3-3
3.4.1 Overview . . . . .	3-3
3.4.2 Gray Level Modification . . . . .	3-3
3.4.3 Hit and Miss Filtering . . . . .	3-7
3.4.4 Region of Interest Extraction . . . . .	3-9
3.5 Indexing . . . . .	3-14
3.5.1 Overview . . . . .	3-14
3.5.2 Indexing Feature Extraction . . . . .	3-14
3.5.3 Indexing Criteria . . . . .	3-15
3.6 Feature Extraction . . . . .	3-16
3.6.1 Overview . . . . .	3-16
3.6.2 Angular Second Moment . . . . .	3-16
3.6.3 Power Spectrum Analysis . . . . .	3-18
3.6.4 Laws Texture Measures . . . . .	3-19
3.7 Prediction . . . . .	3-22
3.7.1 Overview . . . . .	3-22
3.7.2 Feature Selection . . . . .	3-22
3.8 Matching . . . . .	3-23
3.8.1 Overview . . . . .	3-23
3.8.2 Classification . . . . .	3-23
3.8.3 Modified Backpropagation Algorithm . . . . .	3-24
3.9 Summary . . . . .	3-25

	Page
IV. Analysis and Results . . . . .	4-1
4.1 Introduction . . . . .	4-1
4.2 System Development: Training Data Set . . . . .	4-1
4.2.1 Focus of Attention Module . . . . .	4-1
4.2.2 Indexing Module . . . . .	4-4
4.2.3 Feature Extraction and Prediction . . . . .	4-6
4.2.4 Matching . . . . .	4-6
4.3 System Evaluation: Test Data Set . . . . .	4-8
4.3.1 Focus of Attention Module . . . . .	4-8
4.3.2 Indexing Module . . . . .	4-9
4.3.3 Matching . . . . .	4-10
4.4 System Evaluation: Evaluation and Normal Data Sets . . . .	4-11
4.5 Summary . . . . .	4-13
V. Conclusions . . . . .	5-1
5.1 Introduction . . . . .	5-1
5.2 Summary of Methodology . . . . .	5-1
5.3 Summary of Results . . . . .	5-2
5.4 Conclusion . . . . .	5-3
Appendix A. Database Information . . . . .	A-1
Appendix B. Computer Code . . . . .	B-1
B.1 MATLAB Code . . . . .	B-1
B.2 C Code . . . . .	B-28
Bibliography . . . . .	BIB-1
Vita . . . . .	VITA-1



## *List of Figures*

Figure	Page
3.1. Flow Diagram for Microcalcification Detection System . . . . .	3-4
3.2. (a) Sample Mammogram Image	
(b) Histogram of the Image . . . . .	3-5
3.3. (a) Linear vs. Non-Linear Gray Level Mapping	
(b) Effect of Non-Linear Mapping to Mammogram in Figure 3.2 (a). .	3-6
3.4. Spatial Filters: (a) Hit (matched); (b) Box Rim (suppression). . . . .	3-8
3.5. Filter Frequency Response for Hit and Miss Filter with Resulting Difference. . . . .	3-9
3.6. 1-D Cross Section of Effects of Hit & Miss Filters . . . . .	3-10
3.7. Effects of Hit & Miss Filters on Microcalcification Region . . . . .	3-11
3.8. (a) Mammogram after Hit/Miss Filtering	
(b) Histogram of Filtered Mammogram. . . . .	3-12
3.9. Binary Mask Developed from:	
(a) Hit/Miss Thresholding	
(b) Local Thresholding	
(c) Logically "AND" the Two Masks Together . . . . .	3-13
3.10. Laws Masks Used for Indexing:	
(a) L5R5	
(b) L5E5 . . . . .	3-15
3.11. Co-occurrence Matrix Example:	
(a) Image	
(b) $C_\delta$ for $\delta = (1, 0)$ . . . . .	3-17
3.12. (a) Microcalcification ROI and (b) Power Spectrum	
(c) Normal ROI and (d) Power Spectrum . . . . .	3-20
3.13. Microcalcification Tissue: (a) ROI, (b) Binary Mask, (c) L5E5 Filtered ROI	
Normal Tissue: (d) ROI (e) Binary Mask, (f) L5E5 Filtered ROI . . .	3-22
3.14. Basic Neural Network Architecture . . . . .	3-24

Figure	Page
4.1. Sample Images: (a) Full Mammogram (b) Zoom on Microcalcification .	4-2
4.2. Free Response Operating Curve for Varying Global Threshold . . . . .	4-3
4.3. Free Response Operating Curve for Varying Local Threshold . . . . .	4-3
4.4. Free Response Operating Curves using Training Data for:	
(a) Laws Mask L5E5	
(b) Laws Mask L5R5 . . . . .	4-5
4.5. FROC Analysis of Test Data for (a) varying L5R5 LER and (b) varying L5E5 LER . . . . .	4-10

# *List of Tables*

Table	Page
2.1. Criteria for Diagnosis of Microcalcifications[16] . . . . .	2-1
2.2. Risk Factors for Breast Cancer in Women[40] . . . . .	2-2
3.1. Number of Images Available in Database for Various Tissue Abnormalities	3-1
3.2. Non-Linear Gray Level Mapping Improvement to Dynamic Range and Contrast[21] . . . . .	3-7
3.3. Indexing Features and Criteria . . . . .	3-16
3.4. Inner and Outer Ring Radii and Corresponding Object Size . . . . .	3-19
3.5. Power Spectrum Ring Ratios for a Microcalcification ROIs and a Normal ROIs from 14 Sample Images . . . . .	3-19
3.6. Laws Texture Vectors . . . . .	3-20
3.7. Laws Energy Ratios for Micro and Normal ROIs with L5E5 Mask . . .	3-21
4.1. Number of Images and Microcalcification Regions for Training, Testing, Evaluation and Normal Data Sets . . . . .	4-1
4.2. Results of Focus of Attention Module using Training Data . . . . .	4-4
4.3. Fisher Ratio Values and Ranking for each ASM Feature . . . . .	4-6
4.4. Fisher Ratio Values and Ranking for each Laws Energy Ratio Feature Feature . . . . .	4-7
4.5. Fisher Ratio Values and Ranking for each Power Spectrum Analysis Feature . . . . .	4-7
4.6. Training Data Set System Results including Matching Module . . . . .	4-8
4.7. Parameter Settings Determined During System Development . . . . .	4-8
4.8. Results of Focus of Attention Module using Testing Data . . . . .	4-9
4.9. Test Data Set System Results including Matching Module . . . . .	4-11
4.10. Ruck Saliency Values for LER and PSA Feature Sets . . . . .	4-11
4.11. Final System Criteria Used for Evaluation/Normal Data Sets . . . . .	4-12

Table	Page
4.12. System Results on Evaluation and Normal Data Sets . . . . .	4-12
4.13. Average Number of False Regions per Image Reported in Normal Data Set for the Four Feature Sets . . . . .	4-13
4.14. Overall System Results for Each Data and Feature Set . . . . .	4-14
A.1. Training Data Set Information . . . . .	A-2
A.2. Testing Data Set Information . . . . .	A-2
A.3. Evaluation Data Set Information . . . . .	A-3
A.4. Normal Data Set Information . . . . .	A-3

*Abstract*

This research develops and evaluates a novel computer system for the detection of microcalcifications in mammograms using image texture analysis. The system can provide a second opinion to radiologists to decrease the number of false readings, which include diagnosing a mammogram as containing no calcifications when there is (false negative) or as containing microcalcifications when there is not (false positive). The system follows a Model Based Vision (MBV) paradigm for automatic detection of calcifications. The Focus of Attention Module utilizes an image difference technique followed by global and local thresholding to eliminate nearly 90% of the image from further processing. A new, unique feature, the Laws Energy Ratio, is presented. The Laws Energy Ratios from the L5R5 and L5E5 Laws masks provide Indexing criteria which correctly hypothesized 93% of the microcalcification regions while reducing the number of false regions by over 75%. A comparative study of three different texture measures using features calculated from Angular Second Moment, Laws Energy Ratios and Power Spectrum Analysis is presented. Using a neural network trained with a modified backpropagation algorithm, the Power Spectrum Analysis feature set had the best overall performance with an 83% Probability of Detection and an average False ROI Rate of 2.17 ROIs per image over 53 mammograms. A combination of Laws Energy Ratio and Power Spectrum Analysis features selected using Ruck Saliency metrics achieved an 85% Probability of Detection with an average 4 false ROIs per image. Although not specifically developed for classifying regions as malignant or benign, the system correctly identified 89% of the malignant microcalcification regions.

# Computer Aided Detection of Microcalcifications Utilizing Texture Analysis

## *I. Introduction*

Detection of breast cancer is a difficult and, as of yet, unsolved problem. Advances in digital image processing techniques may lead to improvements in detection and diagnosis of this disease. The Air Force Institute of Technology (AFIT) has a long history of applying computer vision and image processing to a host of military related problems[35, 20, 12, 15, 33]. It is the goal of this research to extend this work into the area of medical imaging[17, 25, 9, 13].

### *1.1 Breast Cancer Information*

Breast cancer is a leading cause of cancer deaths among women, currently exceeded only by lung cancer, and will eventually affect one in nine women in the United States[36, 2]. In 1994 alone, the National Cancer Institute (NCI) estimated that 182,000 women would be newly diagnosed with breast cancer, with approximately 46,000 deaths from the disease[3]. The outlook for the next several years does not appear any brighter. The number of newly diagnosed cases is expected to hold steady at approximately 150,000 each year[9].

Mammography is currently the best method for the detection of breast cancer. But in 10-30% of women who have breast cancer, their mammograms were diagnosed as negative. The cancer missed by the radiologist was evident in two-thirds of these mammograms retrospectively[13]. The missed detection may be attributed to a number of factors: the subtle nature of the cancer, poor image quality, eye fatigue or merely oversight by the radiologist. It has been suggested that having the mammograms read by two radiologists may improve detection[22]. This would merely increase the existing high volume workload on the radiologists, possibly leading to more missed cancer regions. Computer aided diagnosis may be a solution to the problem of providing the radiologist with a "second opinion" or a "second reading" by indicating locations of suspect abnormalities in the mammograms.

### 1.2 Computer Aided Diagnosis

Computer aided diagnosis, or CADx, is an automated tool that is based on digital image processing for the detection and classification of breast cancer. The mammographic film can be digitized to allow for the computer processing of the image. The CADx system will consist of basically four main parts:

1. The system would first identify possible cancerous areas, or regions of interest, in the mammogram. This is referred to as Focus of Attention.
2. An initial hypothesis is made as to the classification of the region of interest. This step is referred to as Indexing.
3. The indexed regions are then passed to a set of algorithms to extract features required to verify the initial hypothesis from the indexer. These features will hopefully describe the *critical diagnosis essence* of the image and will be passed on to the final stage of matching.
4. A classifier will attempt to match the extracted features against predicted features to identify the segmented region as normal/abnormal tissue or cancerous/benign tissue.

The CADx system is not being developed to replace the radiologist but to assist them. The primary objective of the system is to improve detection of breast cancer in hopes of increasing the effectiveness and efficiency of mammographic screening[13]. The addition of classifying the suspected regions as cancerous or benign may reduce the number of false-positive diagnoses, thereby decreasing patient morbidity and the number of surgical biopsies performed. The CADx system has the potential to save lives while reducing unnecessary biopsy and surgery.

### 1.3 Problem Statement

Develop a CADx system to detect microcalcifications in a mammogram using an image differencing technique with a global and local thresholding scheme for focus of attention, create an initial indexing hypothesis from cluster and texture analysis information,

extract features based on the texture analysis of the region of interest, and finally match the extracted features using artificial neural networks.

#### 1.4 Scope

Computer algorithms will be developed for the detection and classification of microcalcifications. Microcalcifications are generally the most difficult sign of breast cancer to detect as compared to other signs such as masses or tumors. Microcalcifications are also one of the first mammographically detectable manifestations of cancer.

The Focus Of Attention (FOA) algorithms will be based on image differencing techniques. Work by Chan, *et al.*[8] has demonstrated the potential of this technique. Their technique will be augmented by preprocessing the image to increase the dynamic range of the pixel values where most of the microcalcification information is found. The goal of the FOA stage will be to retain at least 90% of the known cancerous regions while reducing the total number of pixels to be further examined by at least 80%.

Indexing will be accomplished by thresholding the FOA regions of interest (ROIs) based on texture energy ratios and the number of identified microcalcifications in the ROI. Regions passed by the Indexing stage will be assumed to possibly contain microcalcifications. Once this initial hypothesis is generated, a set of features will be extracted from the regions of interest to be matched against predicted features. The predicted features will be developed from training data used during initial development of the system.

The features to be extracted will be a function of second order histogram statistics and image texture analysis. The second order histogram features were based upon previous breast cancer research[17, 9]. The image texture analysis will be based on the use of the Laws Texture measures[30] and Power Spectrum Analysis[41].

The extracted and predicted feature sets will be matched using neural networks. The LNKnet software available here at AFIT will be used. A number of classification techniques are available in LNKnet including K nearest neighbor, Gaussian and Multi-Layer Perceptron (MLP) neural networks[19]. A neural network will also be developed to



evaluate the effects of training on an imbalanced training feature set, or a set where one class has a much larger number of samples available than the other.

### *1.5 Overview*

Chapter I presented the basis for applying computer vision techniques to solving the breast cancer detection problem. Chapter II provides background information on breast cancer, computer vision and related breast cancer research. Chapter III provides methodology of the specific techniques used in this research. Details on the database of mammograms used and analysis of the research are presented in Chapter IV. Final results and conclusions pertaining to this research are given in Chapter V. Additional database information and computer code developed during this research are provided in the appendices.

## II. Background

### 2.1 Breast Cancer

The sign of breast cancer focused on for this research can be identified in a mammogram by small worm-like deposits of calcium, called microcalcifications. It is important to note that calcifications are a normal occurrence in breast tissue. These are referred to as benign calcifications. A radiologist will make a preliminary diagnosis from a mammogram as to the type of calcification using criteria similar to those in Table 2.1[16]. Most calcifications will have characteristics from both the benign and malignant criteria and the radiologist will have to determine the importance of each feature to classify the lesion as more likely to be malignant or benign.

Criteria	BENIGN	MALIGNANT
Size	>0.5mm in diameter	0.1-0.5 mm in diameter
Density	<5 in 1ml vol	≥5 in 1ml vol
Appearance	Regular, smooth shape Large and thick Diffusely scattered, both breasts	Irregular shape, pointed edges Small and Thin Local concentration, one breast

Table 2.1 Criteria for Diagnosis of Microcalcifications[16]

A radiologist may also consider any risk factors that are associated with the patient while making a diagnosis. Age, family history and social status are factors that may be indicators of patients more likely to have malignant lesions. However, these indicators need to be used with care, as the American Cancer Society estimates that 75% of breast cancers occur in women with no high risk factors[1]. Table 2.2 contains an excerpt from a list of common risk factors as compiled by Tanne[40].

Once a suspicious region is detected, a biopsy is normally performed to determine whether the lesion is malignant or benign. The biopsy sample is forwarded to a pathologist to make gross (visible to the naked eye) and microscopic examinations of the sample. Appendix A contains a breakdown of the number of malignant and benign cases used in this study.

Risk Level	Risk Factor	Criteria
Significantly higher risk	Age Country of Birth Family medical history	50 or older North America northern Europe Mother or sister with history of breast cancer
Moderately higher risk	Socioeconomic status Age at first pregnancy Personal medical history Family medical history	Upper class 30 or older Previous cancer in one breast Benign tumor (fibroadenoma) Mother or sister with history of breast cancer
Slightly higher risk	Marital status Place of residence Race  Duration of estrogen exposure  Number of pregnancies Weight Personal medical history	Never married Urban; Northern United States Caucasian women 45 or older African-American women younger than age 40 Menopause after age 55 Menstruation before age 11 None Obesity after menopause Previous endometrial or ovarian cancer

Table 2.2 Risk Factors for Breast Cancer in Women[40]

It is hoped that computer-aided diagnosis can assist a radiologist in detecting suspicious regions in a mammogram and possibly provide a diagnosis of the region based on digital image processing techniques. A promising methodology being developed for automatic target recognition is Model Based Vision(MBV)[4]. This type of architecture will be used for developing the CADx system for this thesis.

## *2.2 Computer-Aided Diagnosis: Model Based Vision*

The Model Based Vision architecture is based on developing hypotheses and testing them to detect and identify objects of interest in an image. The MBV approach utilizes models of sensors, targets and background to better predict the characteristics of potential targets that can be determined by digital image processing. The following provides a brief summary of the stages in an MBV system and related research in those stages.

*2.2.1 Focus of Attention.* The first level of a MBV system is referred to as Focus of Attention(FOA). This stage is often referred to as segmentation. The purpose of this stage is to eliminate as much of the image as possible that obviously does not contain something of interest. For this research, the output of this stage consists of regions where microcalcifications may be present. These regions are referred to as Regions of Interest(ROI). The goal of this stage is to pass all regions containing microcalcifications, or true positives, and as few regions as possible that contain normal tissue, or false ROIs.

A segmentation technique based on image differencing was developed by Chan and Nishikawa[27, 8, 7, 26]. The process is based on filtering the image twice. Once to *increase* the signal to noise ratio (SNR) of the microcalcifications as compared to normal tissue, and the second time to *decrease* the SNR of the microcalcifications. The images are differenced and then globally thresholded to retain only the pixels with values at the high end of the gray-level histogram. These pixels were subjected to local thresholding which retained only pixels with gray levels in the original image that were greater than the mean plus 3.4 times the standard deviation of the surrounding 51 by 51 pixel window. Finally, morphological erosion and a clustering algorithm are applied to reduce the number of false signals. This

technique yielded 85% probability of detection with 2 false regions per image when applied to a set of 78 mammograms.

While the technique developed by Chan and Nishikawa is dependent on local contrast, Brettle, *et al.* created a segmentation scheme that operates in the frequency domain[6]. Operating in the frequency domain allows selected frequency components to be modified independently of spatial contrast. The original image is converted into its frequency components by use of the Fourier Transform. The technique then utilizes a combination of a Butterworth high pass filter and a matched filter tuned to detect structures resembling microcalcifications. The resulting image is spatially filtered to remove noise and globally thresholded to retain only pixels above some multiple of the standard deviation in the image. Brettle applied this technique to 15 segmented regions and achieved 100% probability of detection with a false positive rate of 4 calcifications per region. It should be noted that this technique was not applied to an entire image, only a small portion of a full image. This research will be processing the entire breast image.

Yoshida, *et al.* implemented a set of Least Asymmetric Daubechies (LAD) wavelets for the automated detection of clustered microcalcifications[42]. Their preliminary results using a database of 39 mammograms with 41 microcalcification clusters yielded a detection rate of 85%, with a false positive rate of 5 clusters per image.

*2.2.2 Indexing.* The indexing module creates an initial hypothesis space which attempts to assign some identification to a region of interest in an image. This is an overall likelihood or confidence measure for later model-based refinement. Traditional target recognition schemes do not include this stage, opting to go directly to the next process termed feature extraction.

*2.2.3 Feature Extraction.* The Feature Extraction phase attempts to provide compact, quantitative descriptions of image characteristics. The extracted features are matched against predicted features to recognize targets. There are a number of desirable properties for extracted features[11, 4]:

1. Robust: Reliably found in imagery and stable with respect to small image changes, such as uncertainties in absolute amplitude.
2. Discriminating: Responsive to differences among targets. A trade-off exists between robustness and discriminating power. A system may attempt to classify a region beginning with robust, less discriminating features then use less robust, highly discriminating features to establish fine distinctions.
3. Extractable: Computable from image data.
4. Predictable: Derivable from 3-D models and/or a priori exemplars.
5. Efficient: Low computational load and a minimum set of required features.

The University of Chicago has obtained encouraging results using features derived from the first moment of the power spectrum of the region[13]. Chitre, *et al.* and Kocur have made use of features derived from the second order histogram of the region including: Entropy, Contrast, Angular Second Moment, and Inverse Difference Moments[9, 18]. In further work, Chitre included a set of binary cluster features (number of calcifications, average distance between calcifications, etc.) in addition to the second order histogram features which improved the classification of malignant vs. benign regions[10]. A combination of shape, texture and contrast features were applied to images containing microcalcifications by Parker, *et al.*[28]. Texture features have also been used to discriminate between glandular and fatty regions in a study by Astley and Miller[23]. In their study, the images were filtered with the Laws Texture masks[30] and image statistics were used to classify the breast tissue. The masks found to be most useful were the 5x5 versions of the edge and spot filters (R5R5, L5L5 and S5R5) in discriminating between glandular and fatty regions.

In research accomplished here at AFIT, feature extraction techniques have focused on three main areas: second-order histograms, Karhunen-Loeve transforms and wavelet transforms[17, 18]. Originally developed and evaluated for military and face recognition applications, these techniques were applied to breast cancer detection[25]. The Angular Second Moment(ASM) was generated from the co-occurrence matrix, or second order histogram. In this study, only a single distance vector was used in determining the ASM calculation for the image. The Karhunen-Loeve transform, also referred to as principal

component analysis, attempted to determine the directions of maximum variance in a given feature set. Actual pixel values from malignant and benign regions of interest were used as the feature set. The final area of research applied to breast cancer was wavelet decomposition. Daubechies and biorthogonal wavelet decompositions were applied to the microcalcification regions. The best results were achieved using a biorthogonal wavelet decomposition, obtaining an 88% correct classification rate on 93 difficult to diagnosis images[17].

*2.2.4 Prediction.* The Prediction stage focuses on producing quantitatively correct signature features suitable for matching. This stage may include producing a "model" of a region of interest based on information gained from the Focus of Attention and Indexing stages. This model will attempt to simulate a target in the appropriate background based on image information and will have the same features extracted as the candidate region of interest for use in the matching phase. For this research, the prediction module will not develop models, but will reference training data regions of interest that are consistent with the indexing hypothesis.

*2.2.5 Matching.* Once a region has been processed by the FOA, been assigned an initial hypothesis, and the desired features are extracted from the regions of interest, the features are sent to a classification algorithm in an attempt to verify, or match, the predicted hypothesis. A number of classification schemes have been developed for pattern recognition[11]. Currently, one of the most novel classification schemes for medical imaging is the multilayer perceptron (MLP) artificial neural network[13, 9]. Neural networks have a number of benefits when applied to cancer detection and diagnosis[32]. A neural network, as well as other classifier types, can be evaluated with LNKnet, a versatile classification program[19]. LNKnet is capable of evaluating a given feature set using a number of classifiers, including a statistical (Gaussian) or a non-parametric (K-Nearest Neighbor) classifier.

*2.2.6 Search.* The Search module evaluates the results of the Prediction, Feature Extraction, and Matching process to determine whether or not an acceptable match was

achieved. The search module will examine the output of the match process for this research. The input mammogram images will either contain microcalcifications or will consist of all normal tissue. Therefore, if a region identified as a microcalcification will be deemed an acceptable match.

### 2.3 Feature Selection

In any pattern recognition problem, it is desirable to classify a pattern using as few features as possible[11]. A reduced feature space lends itself to less computational requirements and better generalization to unseen data. A number of techniques are available to attempt to determine which of the features contain the most relevant classification information.

A simple, statistical measure to quantify how separable a feature is in a two class problem is the Fisher Ratio, Eqn 2.1, where  $\mu_i$  and  $\sigma_i$  are the mean and variance of the feature set for class  $i$ [29]. The Fisher Ratio is a measure of the separability of the Probability Density Function(PDF) of the feature for each class. The larger the Fisher Ratio, the more separable the classes are for that particular feature. This test is useful for only a single feature vector and does not give any insight into the effects of combinations of features. Still, it can be used for an initial determination of the potential classification ability for a feature, such as a particular distance vector used to generate an Angular Second Moment value.

$$FR = \frac{(\mu_1 - \mu_2)^2}{(\sigma_1^2 + \sigma_2^2)} \quad (2.1)$$

A technique has been developed that integrates feature and neural network architecture selection by Steppe[38, 39]. The Steppe algorithm uses an iterative likelihood ratio test statistic as a model selection criterion for sequentially determining the “best” neural network.

The Steppe approach is a combination of statistical model building perspective and backwards sequential selection. The process begins with architecture selection, where  $I$  versions of a neural network with  $N$  hidden nodes and  $M$  features are trained and tested. Then, the same number of neural networks are trained and tested with  $N - 1$  hidden nodes.



If the  $N - 1$  hidden node network results are not statistically significantly different than the  $N$  hidden node networks, the reduce network is retained. Next, feature selection is accomplished where  $I$  versions of the current network architecture are trained and tested with  $M$  features. This is followed by  $I$  networks trained and tested with one of the  $M$  features removed. This is done until each feature has been left out. The feature that causes the least statistically significant change in results is eliminated and the process of architecture selection is begun again[39]. This process can be implemented to find the smallest architecture and the single "best" feature or feature subset for a given classification problem[17].

One of the key practical considerations is the necessary computing time and resources for performing architecture and feature selection on a given data set. For large data sets with a number of features, the training of multiple neural networks for each architecture and feature set requires extensive processing time.

Another method designed specifically for neural networks is a derivative based saliency metric developed by Ruck[34]. This saliency metric determines which features effect the output of a trained neural network by taking the derivative of the output with respect to each input feature. The features having the most effect on the output will have a higher value. This is done by training multiple neural networks and averaging the saliency value for each feature. The Ruck method is much faster and easier to implement in comparison to the Steppe algorithm.

## 2.4 Summary

Research in the area of pattern recognition and breast cancer is extensive. A number of candidate techniques have been developed and evaluated yielding promising results. Yet, no single system or technique will be able to correctly identify microcalcification regions in every case. The solution may exist in having a number of techniques processing an image and combining the results. It is the focus of on-going research at AFIT to develop and analyze new techniques for use in diagnosing breast cancer. These techniques are being designed to be implemented in a Model Based Vision architecture. The processes specifically developed in this research are presented and expanded in the next chapter.

### III. Methodology

#### 3.1 Introduction

This chapter describes the actual techniques used to discriminate regions containing microcalcifications from regions of normal tissue.

#### 3.2 Database

The mammograms used in this research were obtained from the Wright-Patterson Medical Center, Wright-Patterson AFB. A total of 72 patient cases were selected to be digitized providing a total of 284 mammograms. The films were digitized to 0.1 mm by 0.1 mm pixel size with 12 bit gray scale resolution(4096 gray levels) using an Lumiscan 200 Laser Film Digitizer and Macintosh computer. The system was calibrated such that the optical density range of 0 to 3.5 was digitized linearly to 0.001 optical density unit/pixel value. After digitizing, each mammogram was manually sized to 1024 x 2048 pixel images for evaluation with the CADx system.

Each mammogram had a corresponding pathology report indicating the diagnosis and location of suspected regions. Dr. Jeff Hoffmeister reviewed and annotated each mammogram as to the location and type of abnormality, if any. Table 3.1 shows the various types of tissue abnormalities and the corresponding number of images available in the database. The total number of images in Table 3.1 exceeds the total number of mammograms digitized as some images contained multiple abnormalities.

Abnormality	Number of Images
Biopsy Proven Malignant Microcalcs	39
Benign Microcalcs	37
Biopsy Proven Malignant Masses	48
Benign Masses	53
No Abnormality Visible	140
<b>TOTAL</b>	284

Table 3.1 Number of Images Available in Database for Various Tissue Abnormalities

### 3.3 System Overview

This section provides a brief overview of the Microcalcification Detection System. A Flow Diagram is shown in Figure 3.1. This system follows the basic Model Based Vision architecture. The first module of the system, Focus of Attention, attempts to reduce the amount of data to be processed by the system. The original image is first preprocessed to improve the contrast and dynamic range of the microcalcifications in the image by remapping the gray levels with a sigmoidal function. This modified image is then filtered with a Hit/Miss technique. The filtered image emphasizes microcalcification-like structures in the image. Regions of Interest, ROIs, are identified by a three step process. First, the filtered image is globally thresholded to retain only the brightest 0.5% of the pixels in the image. Second, the original image is locally thresholded by finding pixels that have a gray level value greater than the mean plus two times the standard deviation of a 51 by 51 pixel box around the pixel of interest. Only pixels surviving both thresholding techniques are retained. Finally, the center coordinates of the minimum number of 64 by 64 pixel ROIs enclosing the retained pixels are determined through a process of ROI centroid migration.

The Regions of Interest passed by the Focus of Attention module are next processed by the Indexing module. This module forms an initial hypothesis as to the type of tissue in the ROI. Three features are extracted from each ROI to develop this hypothesis. The first feature is the number of individual microcalcifications identified in the ROI. The next two features are Laws Energy Ratios, LER, for each ROI. The LER is the ratio of the energy in the microcalcifications only versus the total energy in the ROI after filtering with the L5E5 and L5R5 Laws Masks. ROIs having at least 3 individual calcifications, an L5E5  $LER \geq 0.0287$  and an L5R5  $LER \geq 0.0083$  are given the initial hypothesis of being a region of microcalcifications. These ROIs are then set to the final module, Matching, to confirm the hypothesis.

The Matching module takes the ROIs passed by the Indexing stage and extracts an additional set of features to be used to classify the tissue type as normal or containing microcalcifications. A set of texture features based on Angular Second Moment values, Power Spectrum Analysis and Laws Texture Measures is extracted for each ROI. A neural

network is used to determine if the extracted features best match to tissue containing microcalcifications or normal breast tissue.

Again, the process is shown as a Flow Diagram in Figure 3.1. Each module and the steps contained within that module is shown. The remaining sections will describe in detail each module and the processing involved.

### *3.4 Focus of Attention*

*3.4.1 Overview.* The first step in processing the mammogram image is Focus of Attention (FOA). This stage is often referred to as segmentation. The purpose of this stage is to eliminate as much of the image as possible that obviously does not contain something of interest. The output of this stage consists of regions where microcalcifications may be present. These regions are referred to as Regions of Interest (ROIs). The goal of this stage is to pass all regions containing true abnormalities, or true positives, and as few regions as possible that contain normal tissue, or false ROIs.

There are three steps in the FOA module for this system. The image is first pre-processed to modify the gray levels in an attempt to improve microcalcification contrast and dynamic range. The processed image is filtered using a Hit/Miss filtering technique to identify pixel locations that represent potential microcalcifications. The filtered image is next subjected to a global and local thresholding scheme. The image is globally thresholded to retain only a percentage of the brightest pixels. Those pixel locations are further evaluated by local thresholding those locations in the original image to determine if they are greater than the mean and some multiple of the standard deviation of a small window around the region. Finally, regions of interest are found by grouping surviving pixel locations to retain the minimum number of 64 by 64 pixel regions.

*3.4.2 Gray Level Modification.* After examining a number of sample mammograms containing microcalcifications from the Training Data Set, it was discovered that most of the gray levels containing microcalcification information were in the range of 2200 to 3600. A sample image and its histogram, Figures 3.2(a) and (b), provide an example of how the pixel gray levels associated with background and microcalcifications are

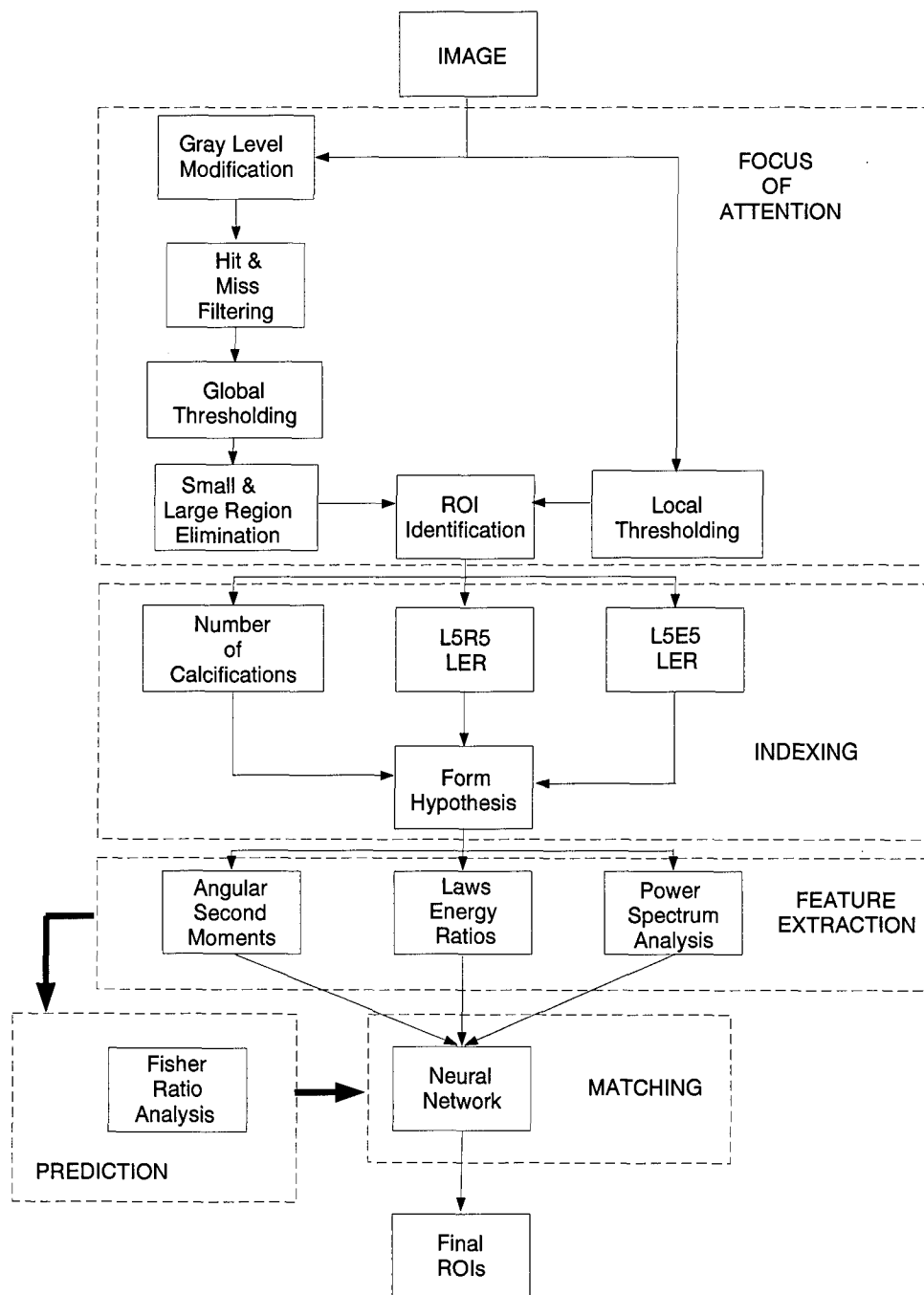
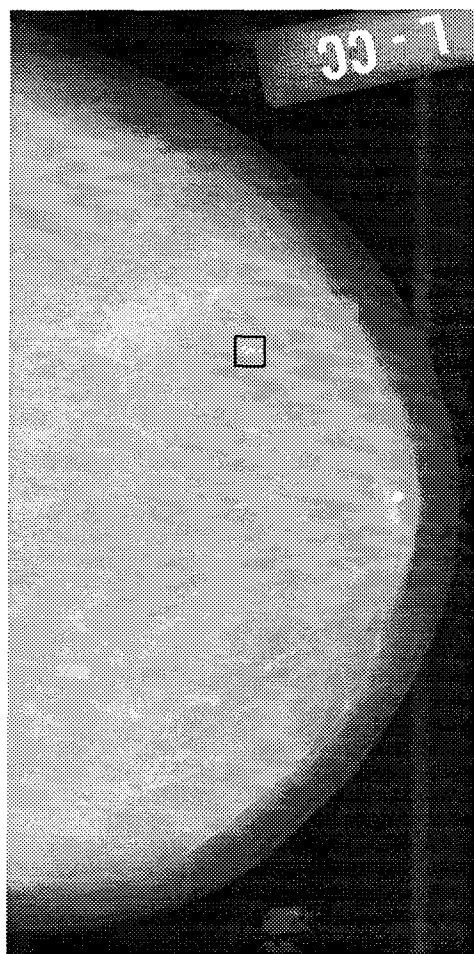
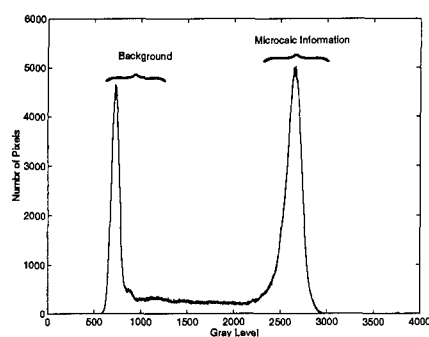


Figure 3.1 Flow Diagram for Microcalcification Detection System



(a)



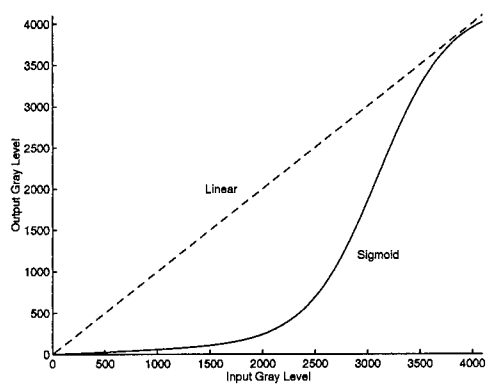
(b)

Figure 3.2 (a) Sample Mammogram Image(b) Histogram of the Image

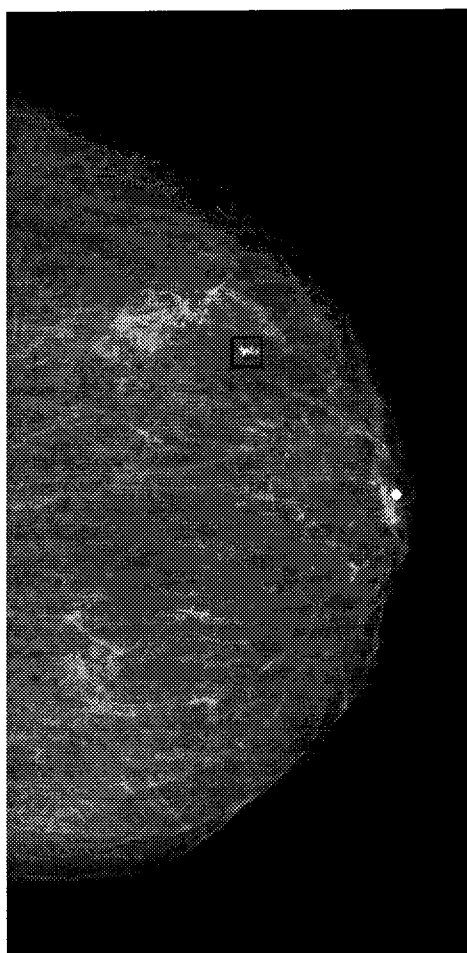
distributed. A non-linear function is applied to the raw image to remap the gray levels of interest such that they occupy a larger range of the available gray levels. Figure 3.3 illustrates the sigmoidal function used to remap the gray levels and the resulting image.

The non-linear mapping has two desirable effects:

- The dynamic range of the microcalcifications regions is increased which also yields improved contrast of the microcalcifications as compared to the surrounding background. To illustrate the increase in dynamic range, a small region containing microcalcifications from fourteen mammograms was extracted from the original and processed images. The dynamic range and contrast was calculated for the regions.



(a)



(b)

Figure 3.3 (a) Linear vs. Non-Linear Gray Level Mapping  
(b) Effect of Non-Linear Mapping to Mammogram in Figure 3.2(a).

Image	Dynamic Range	Contrast
Original	745	0.0463
Processed	1733	0.2060
<b>Improvement</b>	<b>2.37</b>	<b>4.25</b>

Table 3.2 Non-Linear Gray Level Mapping Improvement to Dynamic Range and Contrast[21]

The dynamic range of a region is quantified as  $DR = Max - Min$ , where  $Max$  is the maximum pixel value in the region and  $Min$  is the minimum pixel value. The contrast is quantified using a measure defined by Morrow[24]. The contrast of a region is found by

$$C = \frac{f - b}{f + b}$$

where  $f$  is the mean value of the microcalcification pixels and  $b$  is the mean value of the remaining, or background, pixels. Table 3.2 shows the Dynamic Range and Contrast improvements for the sample regions. The non-linear mapping improved the Dynamic Range by approximately 2.5 and had over a factor of 4 increase in contrast for microcalcification regions.

- The structures that resemble microcalcifications, but have gray levels below 2200, are effectively removed. This helped eliminate a number of false ROIs from being passed to further stages in the Focus of Attention process.

*3.4.3 Hit and Miss Filtering.* A Hit and Miss thresholding technique used in the Focus of Attention stage is modeled after the system developed by Chan and Nishikawa[27, 8, 7]. This technique utilizes two filtered versions of the original image. The first filter, the Hit filter, increases the signal to noise ratio of structures in the mammogram that resemble microcalcifications. The second filter, the Miss filter, reduces the signal to noise ratio of those same structures. A differenced image is obtained by subtracting the Miss filtered image from the Hit filtered image. The differencing removes the majority of the structured background while retaining those regions resembling the targets of interest.

The Hit, or matched, filter used is the three by three kernel shown in Figure 3.4(a). A Box Rim filter, shown in Figure 3.4(b), is used as the Miss filter to suppress the target



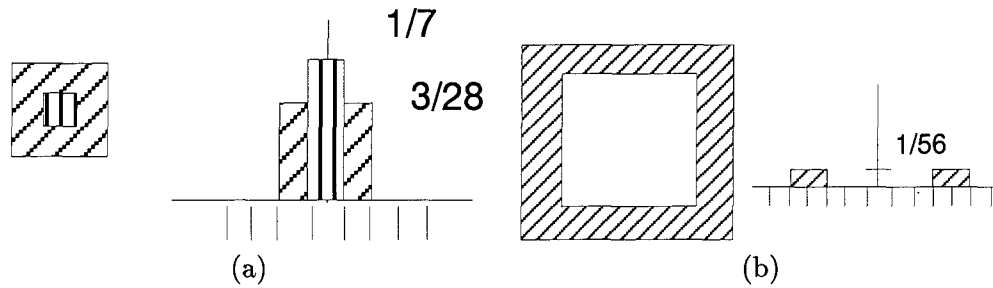


Figure 3.4 Spatial Filters: (a) Hit (matched); (b) Box Rim (suppression).

signal. Previous work by Chan[8] has indicated a filter with an outer dimension of nine pixels and an inner dimension of five pixels yielded the best performance. Chan performed his work on  $100\mu\text{m}$  resolution images, the same resolution as the AFIT database, with a Free Response Operating Curve (FROC) analysis in comparing 6 different Hit/Miss filter combinations.

The frequency response characteristics of the filters are shown in Figure 3.5. Through the differencing processing, the resulting frequency response of the system is a band pass filter. The pass band of approximately 0.15 to 0.45 in normalized frequency ( $\frac{\pi}{8}$  to  $\frac{\pi}{2}$  radial spatial frequency) indicates structures of interest, including microcalcifications, are composed of frequencies in this range. The existence of microcalcifications in this frequency range corresponds to work done by McCandless[21]. His work with wavelet decomposition also indicated a range of  $\frac{\pi}{8}$  to  $\frac{\pi}{2}$  contained frequencies common to microcalcifications.

To demonstrate the effects of the Hit & Miss filter, Figure 3.6(a-d) provides a look at 1-D cross sections from a region containing a microcalcifications and Figures 3.7(a-d) are the actual regions. This sample was taken from image AF055 and has a mass containing microcalcifications. Figure 3.6(a) shows the original region with the microcalcification. Figures 3.6(b) & (c) show the corresponding region after applying the filters. Figure 3.6(d) shows the differenced signal. The same sequence but with the full region is shown in Figures 3.7(a-d). Note how the background mass structure has been reduced to gray scale levels near zero, causing the microcalcifications to be easily thresholded. Defining the Signal to Noise Ratio as the mean value divided by the standard deviation[14],  $SNR = \frac{\text{mean}}{\sqrt{\text{variance}}}$ , the SNR of the original image was 0.0157, hit filtered image - 0.0373, miss filtered image - 0.0249, and the differenced image - 0.3464. The overall effect on the sample mammogram

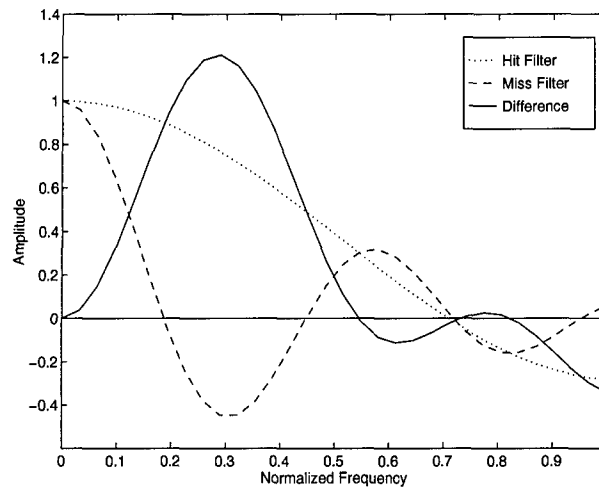
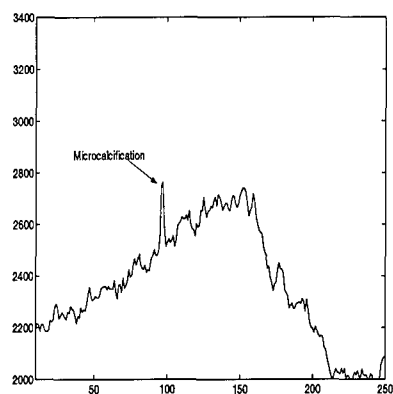


Figure 3.5 Filter Frequency Response for Hit and Miss Filter with Resulting Difference.

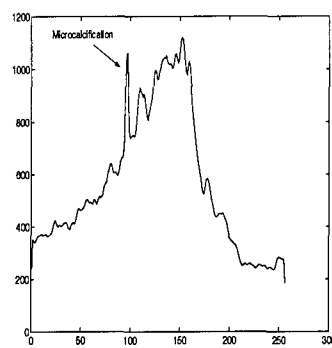
from Figure 3.2(a) is shown in Figure 3.8. Notice how the background has been effectively removed while the microcalcifications have been made more prominent. This is also evident in the histogram of the image, Figure 3.8(b), as the microcalcifications are now comprised of the brightest pixels in the image.

*3.4.4 Region of Interest Extraction.* Once the differenced image is obtained, global thresholding is applied to retain only a percentage of pixels with high gray scale values. The histogram of the differenced image is used to identify the gray scale value where only 0.5% of the pixels have higher values. The pixels that are higher than the threshold are set to one, otherwise the pixels are set to zero. This produces a binary mask image of potential microcalcifications. This binary image is then subjected to a clustering algorithm that identifies groups of connected pixels. Only groups that contain between 3 and 45 pixels are retained. This will eliminate any small or large pixel groups that correspond to noise or other artifacts in the image. This image is later used to extract the microcalcification masks required to generate the texture energy ratios and to determine the number of clusters for each ROI for the Indexing and Matching modules.

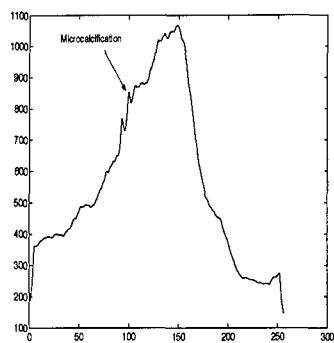
Then, each of the remaining pixels is processed with a local threshold. For each candidate pixel, a 51x51 window is extracted from the original image. The pixel  $g(x, y)$  is



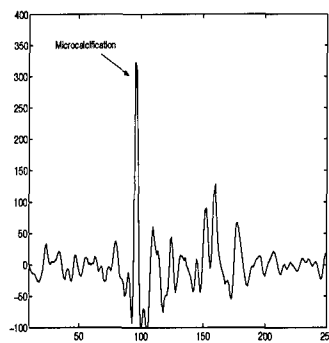
(a) Original Signal



(b) Signal Filtered with Hit Filter

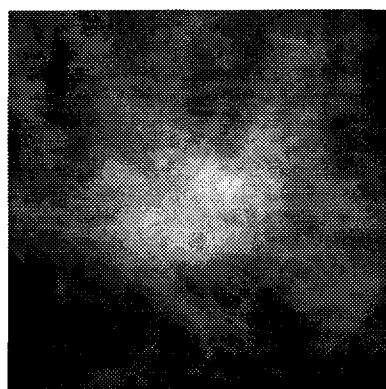


(c) Signal Filtered with Miss Filter

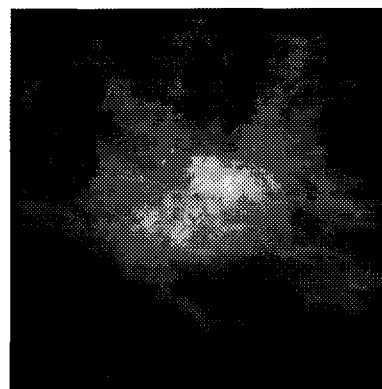


(d) Differenced Signal

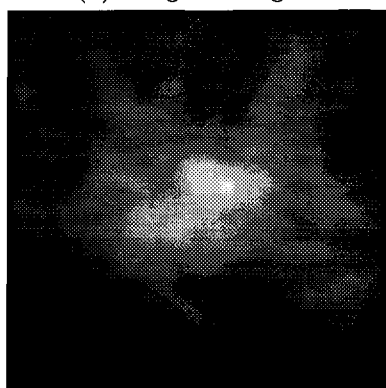
Figure 3.6 1-D Cross Section of Effects of Hit & Miss Filters



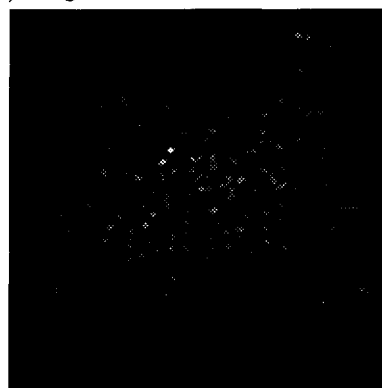
(a) Original Region



(b) Region Filtered with Hit Filter

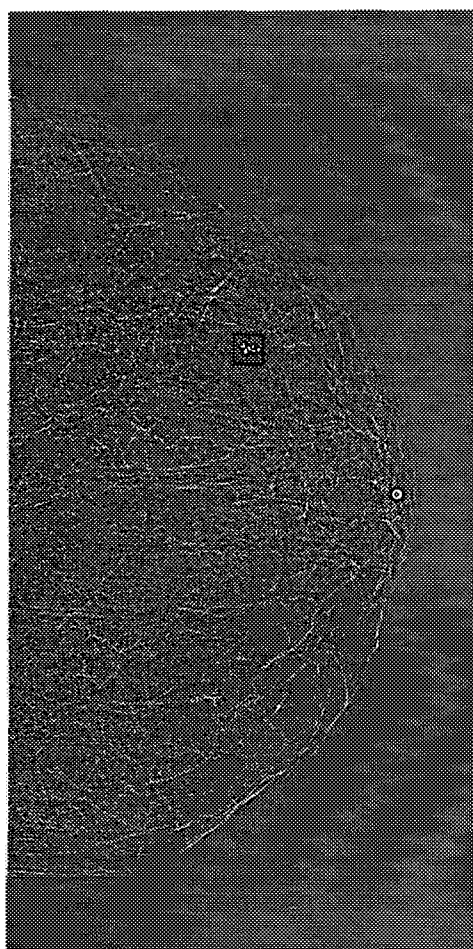


(c) Region Filtered with Miss Filter

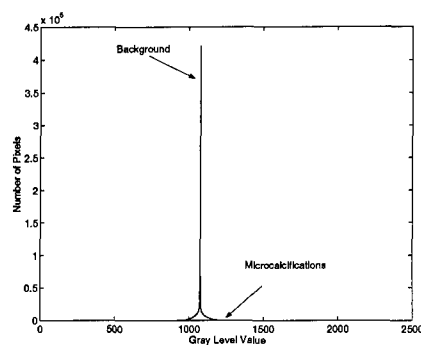


(d) Differenced Region

Figure 3.7 Effects of Hit & Miss Filters on Microcalcification Region



(a)



(b)

Figure 3.8 (a) Mammogram after Hit/Miss Filtering  
(b) Histogram of Filtered Mammogram.

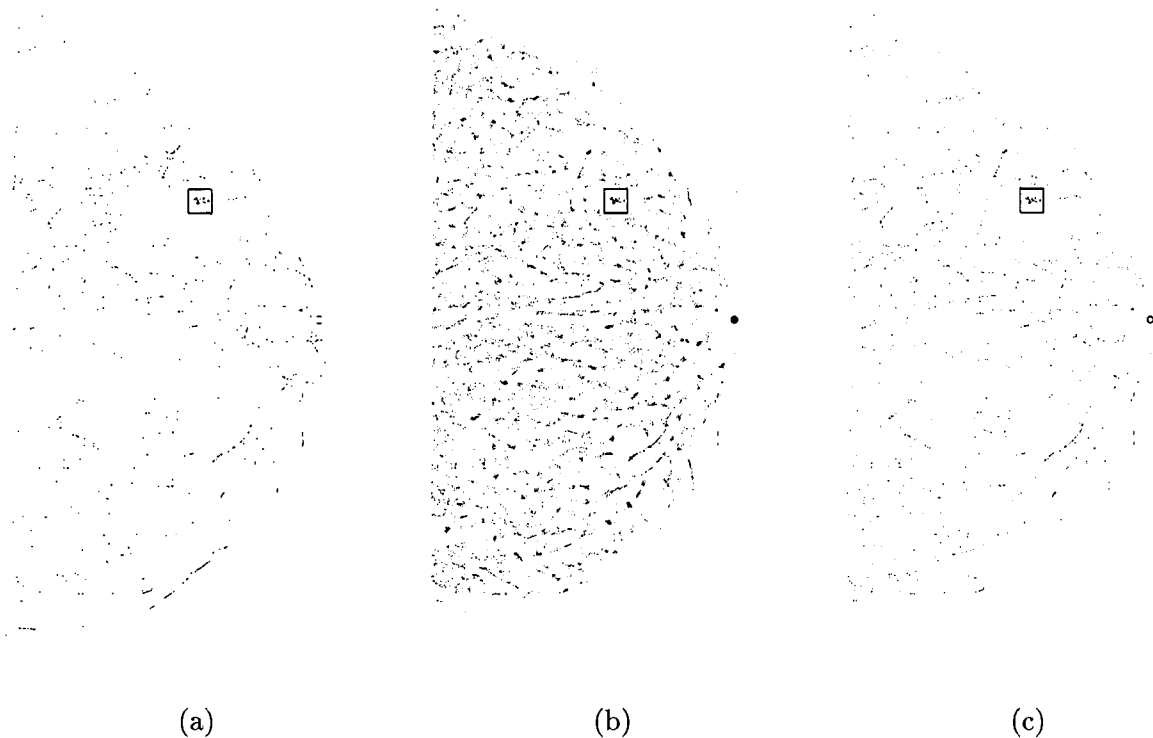


Figure 3.9 Binary Mask Developed from:  
 (a) Hit/Miss Thresholding  
 (b) Local Thresholding  
 (c) Logically "AND" the Two Masks Together

retained only if

$$g(x, y) > \mu + n\sigma$$

where  $\mu$  is the mean value of the local window,  $\sigma$  is standard deviation of the window, and  $n$  is the threshold factor.

The masks developed during the thresholding process can be seen in Figure 3.9(a-c). The first mask is the result of globally thresholding the Hit/Miss filtered image. The second mask is the result of the local thresholding process. By logically "AND"ing the two mask together, only the pixel locations common to both masks are retained. This image is used for ROI selection.

The minimum number of 64x64 boxes that enclose the surviving pixels is next determined. This is accomplished by first finding 512 non-overlapping windows in the image (16 high by 32 wide). The center of mass of each window is calculated and the window is recentered around that point. This process continues until the window moves less than 2 pixels. Overlapping windows are eliminated by comparing the center of mass of each window. If the center of masses of the two windows are within  $d = 20$ , where  $d$  is the Euclidean distance between two window centers, the window with the lowest energy is eliminated. A list of ROI center coordinates is now generated.

At this point, the ROIs are ranked based on the number of pixel locations that correspond to potential microcalcifications. The number of "on" pixels for each ROI location in the binary mask is calculated. True microcalcification ROIs generally have a number of pixel locations identified by the Hit/Miss filtering process as compared to random noise or structures that responded to the filtering.

### *3.5 Indexing*

*3.5.1 Overview.* The Indexing module receives a list of potential microcalcification regions as identified during the Focus of Attention stage. The indexing module forms an initial hypothesis as to the classification of each ROI. In this case, Indexing attempts to further sort out the ROIs with microcalcifications from those containing only normal tissue. In this stage, three features are extracted from each ROI: number of individual calcifications and two Laws Energy Ratios developed from filtering the ROI with a Laws mask.

*3.5.2 Indexing Feature Extraction.* The first feature extracted is the number of individual calcifications as detected by the Hit/Miss filtering operation. An ROI is extracted from the binary image produced by globally thresholding the Hit/Miss filtered image for each coordinate passed by the FOA module. ROIs containing microcalcifications generally have a large number of individual calcifications. This relates to the information used by a radiologist in diagnosing a region containing microcalcifications. Recall Table 2.1 which showed regions of malignant microcalcifications generally contain 5 or more

1	-4	6	-4	1	-1	-2	0	2	1
4	-16	24	-16	4	-4	-8	0	12	4
6	-24	36	-24	6	-6	-12	0	12	6
4	-16	24	-16	4	-4	-8	0	12	4
1	-4	6	-4	1	-1	-2	0	2	1

(a)

(b)

Figure 3.10 Laws Masks Used for Indexing:(a) L5R5(b) L5E5

individual calcifications in a 1 ml volume. The ROIs are 64 x 64 pixel regions with 100 $\mu$ m pixels which gives a 6.4mm by 6.4mm size. For a volume of (6.4mm)<sup>3</sup>, a malignant region of this size would generally contain more than 1.31 individual calcifications. Based on this analysis and observations during system development, ROIs are required to have at least 3 individual calcifications to be given the hypothesis of being a region containing microcalcifications.

The ROIs from the FOA next have two Laws Energy Ratios, as described in detail in Section 3.6.4, calculated using the binary mask used to determine the number of calcifications and the same region location extracted from the original image. From the original image and binary mask ROIs, the indexing stage determines the Laws Energy Ratio, LER, for the L5E5 and L5R5 Laws masks which are shown in Figure 3.10. These two mask were selected during system development for their discriminating ability between regions with microcalcifications from those without for the Training Data Set. Only regions having an L5E5 and L5R5 LER greater than a threshold determined during system development are hypothesized to contain microcalcifications.

*3.5.3 Indexing Criteria.* After processing the Training Data Set images during system development, three indexing criteria were developed as shown in Table 3.3. The first criteria is ROIs must have at least 3 individual calcifications. For the Laws Energy Ratios, it was determined that a L5R5 LER of 0.0083 and a L5E5 LER of 0.0346 or greater was appropriate for separating microcalcifications from normal tissue in the Training Data Set. Any ROI meeting this criteria is assigned an initial hypothesis of being a region of microcalcifications. These regions are now sent to the Matching Module to confirm or reject this hypothesis.



Index Feature	Criteria
Number of Clusters	$\geq 3$
L5R5 LER	$\geq 0.0083$
L5E5 LER	$\geq 0.0346$

Table 3.3 Indexing Features and Criteria

### 3.6 Feature Extraction

*3.6.1 Overview.* The ROIs given an initial hypothesis of being a region of microcalcifications are passed to the Feature Extraction module which processes the region in an attempt to provide a quantitative description of image characteristics that can be used by a classifier to discriminate between microcalcification and normal tissue regions. Three different texture metrics are examined for their ability to extract the “diagnosis essence” of the ROI:

- Angular Second Moment
- Power Spectrum Analysis
- Laws Energy Ratios

Each technique is discussed in detail in the following sections.

*3.6.2 Angular Second Moment.* Angular Second Moment, ASM, is a measure often used to classify images based on texture analysis. The ASM value is based on gray level co-occurrences, i.e., on joint probability densities of pairs of gray levels. Let  $\delta = (\Delta x, \Delta y)$  be a vector in the  $(x, y)$  plane. For any such vector and image  $f(x, y)$ , the joint probability density of the pairs of gray levels that occur at points separated by  $\delta$  can be found. This joint density takes the form of a matrix,  $C_\delta$ , commonly referred to as the gray level co-occurrence matrix, where  $C_\delta(i, j)$  is the probability of the pair of gray levels  $(i, j)$  occurring at a vector separation  $\delta$ . The co-occurrence matrix is  $m$  by  $m$ , where  $m$  is the number of possible gray levels.

It is easy to compute the  $C_\delta$  matrix for a given image by counting the number of times each pair of gray levels occur at a vector separation  $\delta = (\Delta x, \Delta y)$ , where  $\Delta x$  and  $\Delta y$  are integers. The following example illustrates the  $C_\delta$  matrix is developed for  $\delta = (1, 0)$ .

0	1	2	4
3	0	1	2
4	1	4	4
0	1	0	1

(a)

0	1	0	1	0
1	1	0	0	1
0	1	0	0	1
0	0	0	0	1
2	1	1	0	0

(b)

Figure 3.11 Co-occurrence Matrix Example:(a) Image(b)  $C_\delta$  for  $\delta = (1, 0)$

Weszka, et al., in their study of texture measures for the classification of terrain, point out:

If a texture is coarse, and  $\delta$  is small compared to the sizes of the texture elements, the pairs of points at separation  $\delta$  should usually have similar gray levels. This means that the high values in the matrix  $C_\delta$  should be concentrated on or near its main diagonal. Conversely, for a fine texture, if  $\delta$  is comparable to the texture element size, then the gray levels of points separated by  $\delta$  should often be quite different, so that the values in  $C_\delta$  should be spread out relatively uniformly. Thus a good way to analyze texture coarseness would be to compute, for various values of the magnitude of  $\delta$ , some measure of the scatter of the  $C_\delta$  values around the main diagonal[41].

Similarly, texture directionality can be analyzed by comparing the spread measures of  $C_\delta$  for various directions of the vector  $\delta$ .

$$ASM = \sum p(i, j)^2 \quad (3.1)$$

The Angular Second Moment calculation is defined in Equation 3.1. In this form,  $p(i, j)$  is defined as

$$p(i, j) = \frac{C_\delta(i, j)}{\sum_x \sum_y C_\delta(x, y)}$$

This measure is smallest when each  $p(i, j)$  are as equal as possible and large when some elements are large and others small, such as when the values are largely concentrated around the main diagonal. For the example  $C_\delta$  matrix in Figure 3.11, the ASM value is 0.0972.

Previous work by Kocur[17] and Chitre[9, 10] classified benign and malignant microcalcifications using texture features, specifically, Angular Second Moment. In both studies, only a single value of  $\delta$  was used in constructing the  $C_\delta$  matrix. A better representation

of the true texture present in the microcalcification region of interest may be gained by evaluating multiple values of  $\delta$  in order to determine texture coarseness and directionality. This measure will be used to separate normal tissue ROIs from ROIs containing microcalcifications.

**3.6.3 Power Spectrum Analysis.** The Fourier transform of an image  $f(x, y)$  is defined by Equation 3.2 and the Fourier power spectrum is  $|F|^2 = FF^*$  (where  $*$  is the complex conjugate).

$$F(u, v) \equiv \int_{-\infty}^{\infty} \int_{-\infty}^{\infty} e^{-j2\pi(ux+vy)} f(x, y) dx dy \quad (3.2)$$

The radial distribution of values in  $|F|^2$  is sensitive to texture coarseness in  $f(x, y)$ [41]. A region of coarse texture will have high values concentrated near the origin, while fine texture regions will have values of  $|F|^2$  more spread out. A method to analyze texture properties of an image using this fact is to find the averages of  $|F|^2$  taken over ring-shaped regions centered at the origin, as given by Equation 3.3 for various values of the ring radius  $r$ , where  $r = \sqrt{u^2 + v^2}$  and  $\theta = \tan^{-1} \frac{v}{u}$ [41].

$$\phi_r = \int_0^{2\pi} |F(r, \theta)|^2 d\theta \quad (3.3)$$

Since the regions analyzed in this research are  $n$  by  $n$  digital images, the discrete Fourier transform is used and the texture features from the power spectrum,  $\phi_{r_1, r_2}$ , are calculated by Equation 3.4.

$$\phi_{r_1, r_2} = \sum_{\substack{u^2+v^2 < r_2^2, u, v \leq n-1 \\ u^2+v^2 \leq r_1^2, u, v \geq 0}} F(u, v) \quad (3.4)$$

Various values of the inner and outer ring radii  $r_1$  and  $r_2$  are selected to correspond with frequency limits of various size objects. For the 64 by 64 ROIs being generated by the Hit/Miss filtering stage, rings investigated and the corresponding object size are listed in Table 3.4.

$r_1, r_2$	Object Size (pixels)
[0,1]	32
(1,2]	16
(2,4]	8
(4,8]	4
(8,16]	2
(16,31]	1

Table 3.4 Inner and Outer Ring Radii and Corresponding Object Size

Ring	Micro ROI		Normal ROI	
	Mean	Std	Mean	Std
[0,1]	0.5956	0.0728	0.6159	0.0569
(1,2]	0.0241	0.0098	0.0230	0.0096
(2,4]	0.0441	0.0144	0.0411	0.0129
(4,8]	0.0705	0.0206	0.0582	0.0133
(8,16]	0.1049	0.0221	0.0916	0.0136
(16,32]	0.1410	0.0199	0.1480	0.0186

Table 3.5 Power Spectrum Ring Ratios for a Microcalcification ROIs and a Normal ROIs from 14 Sample Images

Sample regions of microcalcifications and normal tissue with their corresponding power spectrum are shown in Figure 3.12. Notice how the power spectrum of the microcalcification image is more concentrated in the low frequency values. This is reflected in the ring ratios as the fraction of energy in the lower frequencies is higher for the microcalcifications, as shown in Table 3.5.

**3.6.4 Laws Texture Measures.** A set of texture features based on the correlation of pixel neighborhoods with a set of standard masks was developed by Laws[30]. The masks are derived from three simple vectors:  $L3$  [1 2 1],  $E3$  [-1 0 1] and  $S3$  [-1 2 -1]. The vectors represent one-dimensional operations of center-weighted local averaging, symmetric first (“edge detection”) and second (“spot detection”) differencing. By convolving these vectors with themselves and each other, five vectors are developed which are listed in Table 3.6.

By taking the outer product of every combination of vectors, twenty five 5x5 texture “masks” are created. Each mask is convolved with an image and the statistics of the resulting image, such as the sums of the squared or absolute values of each pixel, is used

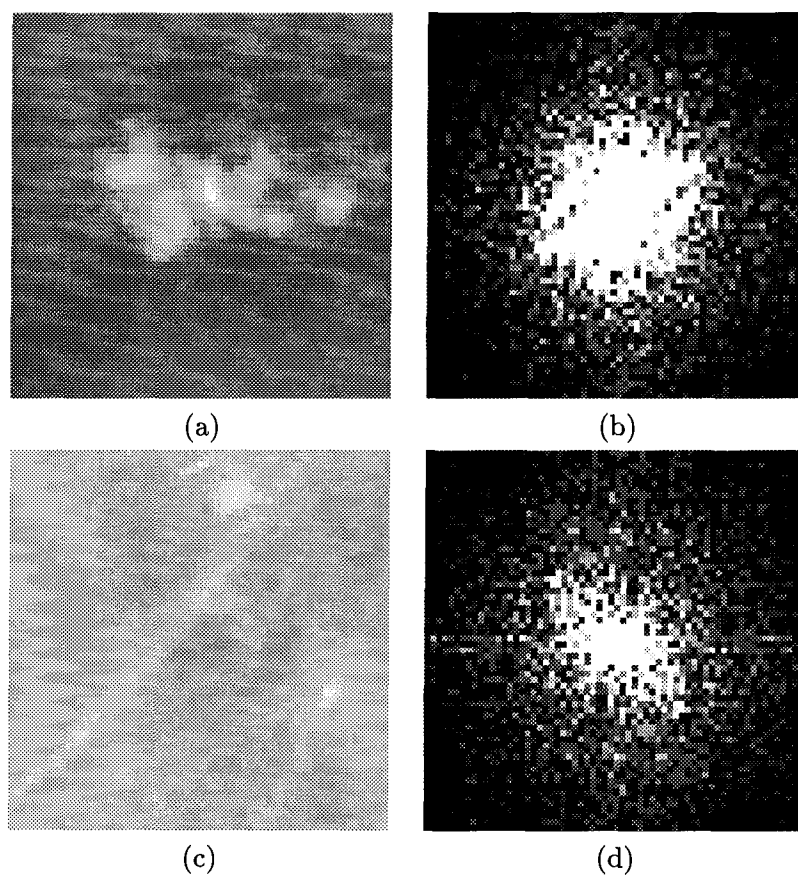


Figure 3.12 (a) Microcalcification ROI and (b) Power Spectrum  
(c) Normal ROI and (d) Power Spectrum

Label	Result of	Vector	Description
$L5$	$L3 * L3$	[1 4 6 4 1]	Local Average
$S5$	$E3 * E3$	[-1 0 2 0 -1]	Spot Detector
$R5$	$S3 * S3$	[1 -4 6 -4 1]	Ripple Detector
$E5$	$L3 * E3$	[-1 -2 0 2 1]	Edge Detector
$W5$	$E3 * S3$	[-1 2 0 -2 1]	Wave Average

Table 3.6 Laws Texture Vectors

ROI Type	L5E5 LER	
	mean	std
Microcalcification	0.0842	0.0498
Normal Tissue	0.0128	0.0201

Table 3.7 Laws Energy Ratios for Micro and Normal ROIs with L5E5 Mask

to define the texture properties of the image. This results in a texture energy measure of the image.

For this research, all twenty five masks are investigated to determine which, if any, respond strongly to regions containing microcalcifications while having little effect on normal tissue areas. The Laws features are calculated for regions detected by the Hit/Miss filtering. A ratio of texture energy is calculated for each region of interest and each texture mask. This ratio is defined in Eqn 3.5, where  $LER$  is the Laws Energy Ratio,  $E_{Micros}$  is the energy in the laws filtered image corresponding to the possible microcalcifications, and  $E_{Total}$  is the total energy in the laws filtered image.

$$LER = \frac{E_{Micros}}{E_{Total}} \quad (3.5)$$

$E_{Micros}$  is determined by summing only the pixel values in the ROI that correspond to the pixels in the binary mask developed during the FOA module.  $E_{Total}$  is the sum of all pixel values in the ROI.

Figure 3.13 shows the results of filtering two ROIs with the Laws mask L5E5. The center images are the binary mask showing the areas corresponding to possible microcalcifications as detected by the FOA module. Notice how the filtered image of the microcalcifications have the majority of the energy concentrated in the areas found in the binary masks. This results in a high LER. The false ROI filtered images have energy more evenly distributed throughout the image which results in a lower LER. The mean and standard deviation for the L5E5 LER for the ROIs identified in the Training Data Set are listed in Table 3.7.

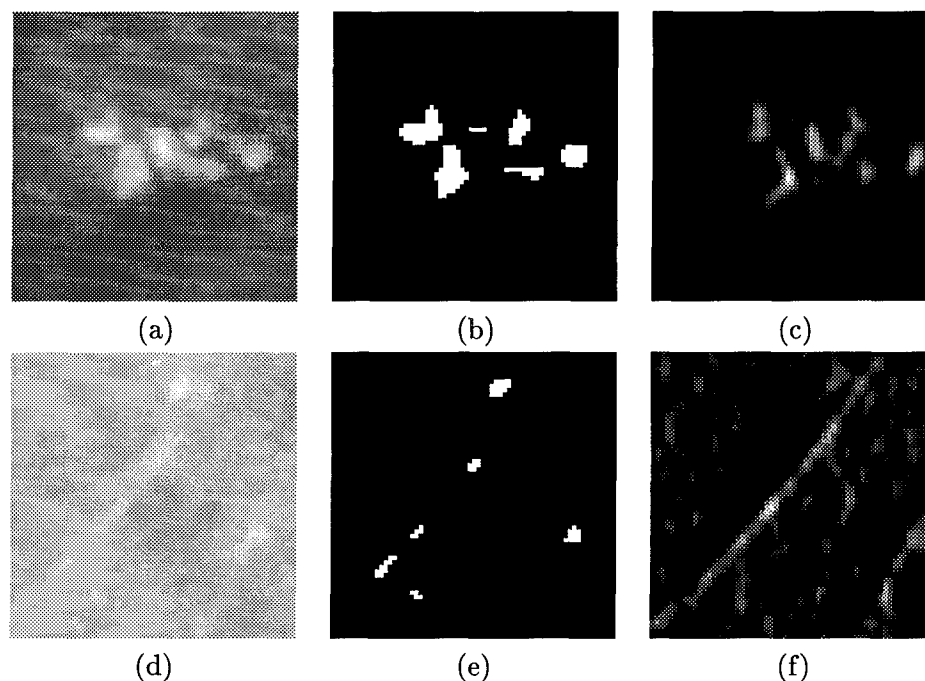


Figure 3.13 Microcalcification Tissue: (a) ROI, (b) Binary Mask, (c) L5E5 Filtered ROI  
Normal Tissue: (d) ROI (e) Binary Mask, (f) L5E5 Filtered ROI

### 3.7 Prediction

**3.7.1 Overview.** The Prediction Module in a Model Based Vision System produces quantitatively correct “signature” features suitable for matching. These features are used to match those obtained by the Feature Extraction module. For this research, the prediction module does not develop a model, but references features obtained during system development from training data. These features are used to train the neural network used in the Matching module. From known microcalcification and normal tissue regions, the three different texture measures (ASM, Power Spectrum Analysis, and Laws Energy Ratios) are calculated. This results in a total of 56 different features for each training region. In an effort to reduce the training feature space, feature selection is done based on Fisher Ratio analysis.

**3.7.2 Feature Selection.** In any pattern recognition problem, it is desirable to reduce the number of features used in classifying a set of data. This reduces computational requirements while usually improving the generalization of the classifier. The trick is to

find out *which* of the available features are the discriminatingly relevant features, that is, best separate one class from another. The Fisher Ratio is a simple, statistical measure to quantify the separation of two classes for a single feature. Recall, the Fisher Ratio is given by

$$FR = \frac{(\mu_1 - \mu_2)^2}{(\sigma_1^2 + \sigma_2^2)}$$

For each feature, the F-ratio is calculated. The features with the highest F-ratios are used for matching. The number of features that can be used are determined in the next section, Matching.

### 3.8 Matching

*3.8.1 Overview.* ROIs surviving the Focus of Attention and Indexing stage are assigned an initial hypothesis of being a region of microcalcifications. The Matching Module attempts to confirm or reject this hypothesis by using the information provided by the Feature Extraction and Prediction Modules to discriminate between microcalcification and normal tissue. The features used by the classifier are selected based on the Fisher Ratio calculation in an attempt to identify the more discriminatingly relevant features. These features are used by a single hidden layer neural network to perform the classification. The neural network is trained using a modified backpropagation algorithm to reduce training time. The following sections review in detail the methods used.

*3.8.2 Classification.* A single hidden layer neural network with one output node, as shown in Figure 3.14, is used for classifying the ROIs using the extracted features. The neural network is trained using a batch backpropagation algorithm to adjust the weights. The network outputs are clamped to  $1 - \epsilon$  for any value greater than  $1 - \epsilon$  and to  $\epsilon$  for values less than  $\epsilon$  during training to reduce the likelihood of the network getting stuck in a local minima[37].

The number of input nodes,  $I$ , is the number of features. This value is determined using Foley's Rule[31] which requires at least three times the number of training samples per class for each feature. Since there are only 18 microcalcification samples in the training set, a maximum of 6 features are used. The number of hidden nodes,  $L$ , allowed is determined



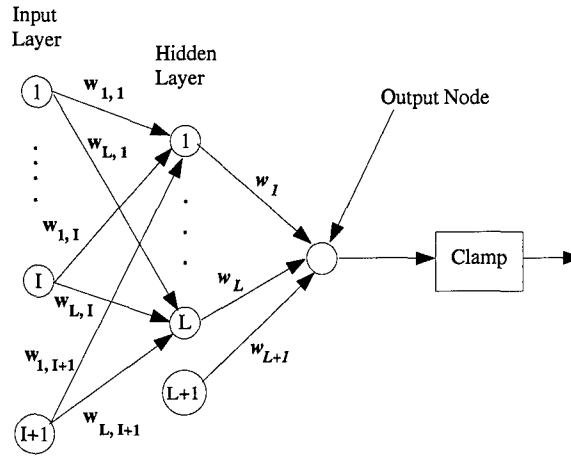


Figure 3.14 Basic Neural Network Architecture

using Cover's Rule[31] which states

$$L = \frac{\frac{1}{2}N - 1}{I + 1}$$

where  $N$  is the number of samples in the training. With 99 samples in the training set and 6 features, this yields a maximum of approximately 7 hidden nodes. Foley's and Cover's rules give a good starting place as to the proper architecture for a neural network, but are not set in stone. An architecture exceeding these values can be used, if an independent test set is held out to verify the neural net performance.

From the Prediction Module Feature Selection, the top 6 features based on F-ratio analysis are used for training and testing of the neural network. To examine the effects of various architectures, the number of hidden nodes is varied from 1 to 9. Two data sets, Evaluation and Normal Data Sets, are with held to verify the classification performance of the Matching Module.

**3.8.3 Modified Backpropagation Algorithm.** One of the difficulties in applying a classification scheme to the breast cancer problem is the lack of samples in one or both classes. There are generally a larger number of normal tissue samples than abnormal. This is a major disadvantage for a backpropagation trained neural network, as the convergence of the net output error is very slow[5]. This occurs when the negative gradient vector

computed by backpropagation actually *increases* the error for the subordinate class during the initial iterations.

A solution to this problem is to calculate a direction in the weight space that is downhill in *both* the dominant and subordinate classes. Anand, *et al.*[5], recommend finding a descent vector  $v$  which satisfies Equation 3.6.

$$-v \cdot \nabla E_c(W) < 0, \quad c = 1, 2 \quad (3.6)$$

This vector takes the place of the gradient vector in the backpropagation algorithm, Equation 3.7, where  $W(k)$  is the collection of weights in the neural network at the beginning of the  $k$ th iteration,  $\lambda$ , a positive constant, is the learning rate and  $\nabla E(W) = \sum \nabla E_c(W)$ ,  $c = 1, 2$ .

$$W(k+1) = W(k) - \lambda \nabla E(W) \quad (3.7)$$

The direction of  $v$  is set to bisect the angle between  $-\nabla E_1(W)$  and  $-\nabla E_2(W)$ , the gradients of the error vector for class 1 and 2, respectively. This is accomplished by finding  $v$  using Eqn 3.8. The magnitude of  $v$  is set to be the same magnitude as would of been computed by the standard backpropagation, as in Equation 3.9.

$$v = \frac{1}{2} * \left( \frac{-\nabla E_1(W)}{\|-\nabla E_1(W)\|} + \frac{-\nabla E_2(W)}{\|-\nabla E_2(W)\|} \right) \quad (3.8)$$

$$\|v\| = \|\nabla E_1(W) + \nabla E_2(W)\| \quad (3.9)$$

This modified backpropagation algorithm is used to train the neural networks in hopes of reaching a converged network more rapidly that has minimum error in both classes.

### 3.9 Summary

The Model Based Vision architecture is used to develop the microcalcification detection system. The Focus of Attention module uses a Hit/Miss filtering technique followed by global and local thresholding to select possible Regions of Interest (ROIs). The Indexing

Module uses information from two Laws Energy Ratios and the number of individual calcifications in the ROI in assigning the initial hypothesis. The Feature Extraction Module obtains texture features using three different techniques: Angular Second Moment, Laws Energy Ratios, and Power Spectrum Analysis. The top 6 features based on Fisher Ratios determined during the Prediction Module are retained for use in the Matching Module. The Matching Module uses a modified backpropagation algorithm Multilayer Perceptron Neural Network to classify the ROI as containing microcalcifications or normal tissue. The results obtained from testing on the AFIT database are provided in the next chapter.

## IV. Analysis and Results

### 4.1 Introduction

The microcalcification system was developed and evaluated using three separate data sets. The first data set, labeled Training Data Set, was used to initially develop the system and determine thresholding levels and indexing criteria values used in the Focus of Attention and Indexing Modules. The second data set, Test Data Set, was used to verify the accuracy of the thresholds determined during training. Analysis of the results from the test set were used to adjust threshold values before going on to the final data set. Once all parameters and thresholds have been determined using the training set and slightly modified to improve accuracy on the test set, a final data set, the Evaluation Data Set, was used to verify the detection capability of the system on unseen data. This was a "sanity check" to determine if the system was over tuned to the data used for development. The results from the Evaluation Data set should be a reasonable indication of the performance of the system to any image data set. An additional data set, Normal Data Set, made up of images with no radiologist noted abnormalities, was used to evaluate how the system performs for images containing no diagnosed microcalcifications. The number of images and true regions of interest for each data set is listed in Table 4.1. Additional details concerning the data sets used can be found in Appendix A.

### 4.2 System Development: Training Data Set

*4.2.1 Focus of Attention Module.* The Focus of Attention module was initially evaluated using the 14 mammograms making up the Training Data Set. Each image had

Data Set	Number of Images	Number of Microcalcification Regions
Training	14	18
Testing	17	20
Evaluation	12	16
Normal	10	0
<b>Total</b>	<b>53</b>	<b>54</b>

Table 4.1 Number of Images and Microcalcification Regions for Training, Testing, Evaluation and Normal Data Sets

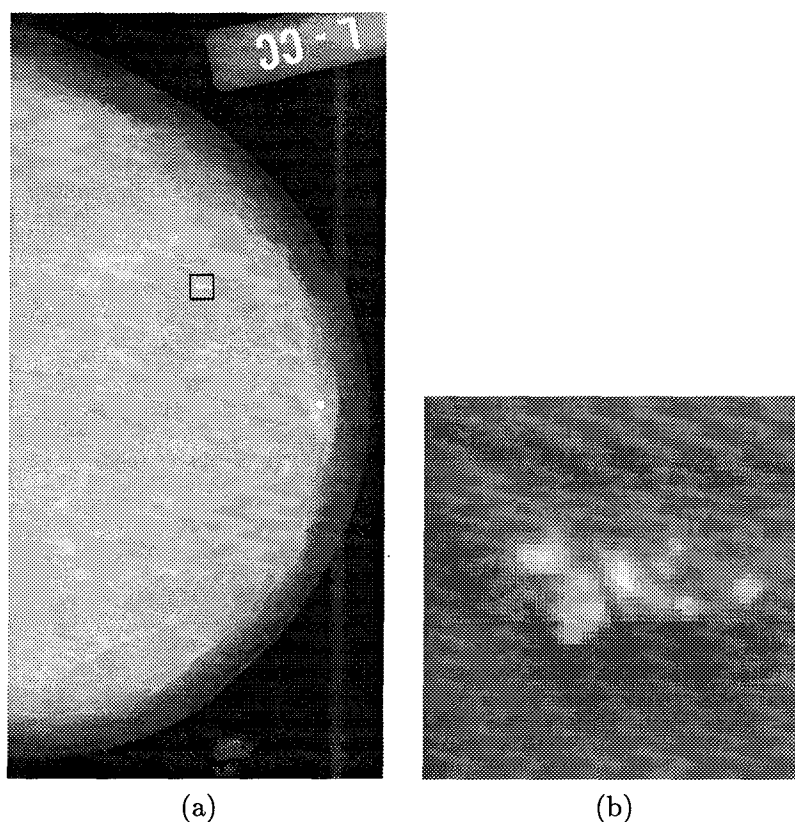


Figure 4.1 Sample Images: (a) Full Mammogram (b) Zoom on Microcalcification

a radiologist noted and biopsy confirmed malignant or benign microcalcifications. The microcalcifications in each image varied from very high to low contrast in comparison to the surrounding background. Figure 4.1 provides an example of the mammogram images used in this study and a close-up of the microcalcification present in the image.

Each training image was first processed by the FOA module to identify the proper thresholds for the global and local thresholding stages. Each training image was processed multiple times as the two parameters were varied independently - the percentage of pixels passed in global thresholding and the multiplicative factor of the standard deviation in the local thresholding. The first parameter that was varied was the top percentage of pixels passed by the global thresholding stage. While this parameter was varied from 0.2% to 0.5%, the multiplicative factor was held constant at a value of 2.0. The multiplicative factor was then varied from 1.0 to 2.5 as the top percentage of pixels was held constant to a value of 0.3%. Figures 4.2 and 4.3 show the results obtained from the 14 test images presented

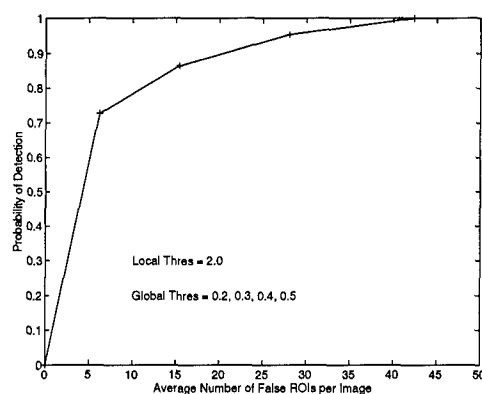


Figure 4.2 Free Response Operating Curve for Varying Global Threshold

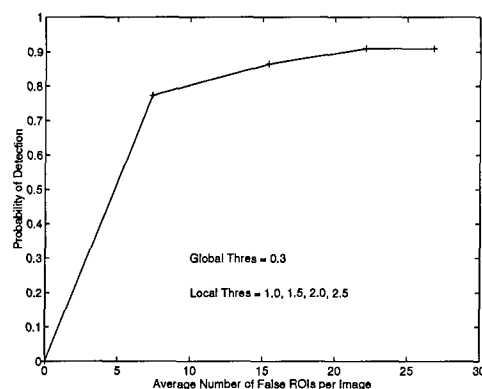


Figure 4.3 Free Response Operating Curve for Varying Local Threshold

as Free Response Operating Curves(FROC). The FROC shows the percentage of correctly segmented regions versus the number of false ROIs per image. The ideal operating point is the upper left corner of the plot which indicates the correct regions are being identified with a minimal number of false regions being retained.

By allowing the top 0.5% of pixels in the differenced image to pass the global thresholding and a multiplicative factor of 2.0 in the local thresholding, 100% of the microcalcification regions in the 14 test images can be identified with approximately 45 false ROIs per image. The goal of this stage is to pass all of the potential regions on to the Indexing module, which attempted to further reduce the false regions while retaining the true regions containing microcalcifications. The number of correct regions identified, their ranking based on number of "on" pixels in the binary mask ROI, and the total number of regions found for each training image is shown in Table 4.2. Note that except for one region

Image	Number of Correct Regions	Rank	Total Number of Regions
AF005	2/2	1, 2	59
AF006	3/3	1, 2, 5	66
AF007	2/2	1, 2	49
AF008	1/1	13	17
AF009	1/1	1	21
AF020	1/1	7	39
AF022	1/1	1	66
AF024	1/1	1	38
AF033	1/1	2	41
AF038	1/1	1	75
AF040	1/1	5	33
AF045	1/1	1	35
AF047	1/1	4	25
AF055	1/1	7	30
<b>Total</b>	18/18	3.17 (mean)	594

Table 4.2 Results of Focus of Attention Module using Training Data

in image AF008 which ranked 13th out of 17, all the remaining regions were ranked within the top 7 regions. The system could pass only the top 7 ROIs based on this ranking and have an acceptable Probability of Detection of 95.4% and an average False ROI Rate of 5.93 regions per image. To improve this performance, the Indexing and Matching Modules are used to reduce the False ROI Rate.

*4.2.2 Indexing Module.* The indexing module received the list of ROI center coordinates from the Focus of Attention Module. A 64 by 64 region from the FOA binary mask and the original image was extracted for each of the coordinates. The binary mask was used to determine the number of individual calcifications in each ROI. After processing the 14 training images, the regions containing microcalcifications had at least three individual calcifications present. This was assigned as the first indexing criteria.

For the ROIs containing at least three individual clusters, each ROI from the original image was filtered with each of the 25 Laws masks. The Laws Energy Ratio, LER, was calculated for each ROI/Laws mask combination. This ratio determines the energy contained in the individual calcifications versus the total energy in the ROI filtered by the Laws Mask. To determine which of the Laws Energy Ratios had the strongest response

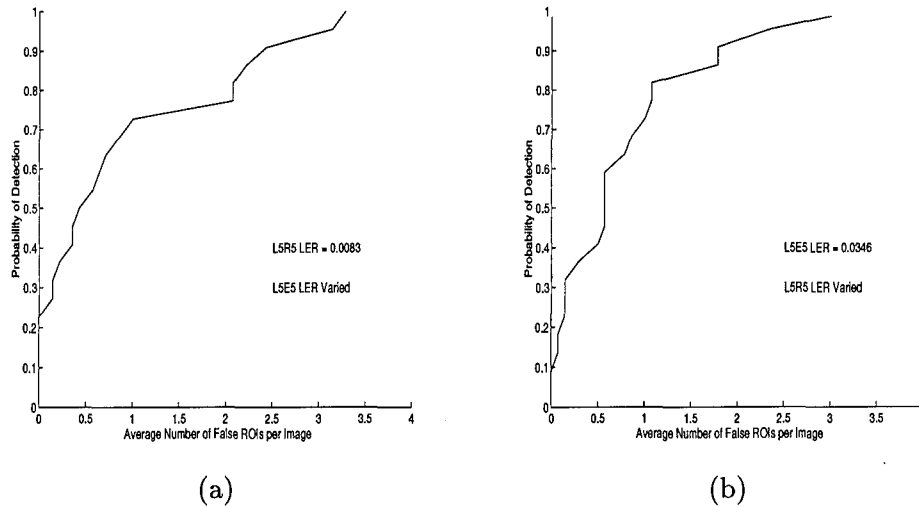


Figure 4.4 Free Response Operating Curves using Training Data for:  
 (a) Laws Mask L5E5  
 (b) Laws Mask L5R5

to the microcalcifications, a FROC analysis was done for each of the 25 LERs. The Laws Masks L5E5 and L5R5 had 100% Probability of Detection with the lowest False ROI Rate for the 14 training images, as shown in Figures 4.4(a) and (b).

The Indexing module analysis on the 14 training images provided a first attempt at setting the proper thresholds for the LER for mask L5E5 and L5R5. From the FROC analysis, only ROIs with L5E5 LER of greater than 0.0346 and an L5R5 LER of greater than 0.0083 were given the initial hypothesis of being a region of microcalcifications. For the 14 training images, this resulted in a 100% Probability of detection and an average of 3.2 False ROIs per image. This is comparable to other researchers results. Recall the performance achieved by the system developed by Chan[27] which obtained an 85% Probability of Detection rate with 2 false regions per image and Yoshida[42] with 83%  $P_D$  and 5 false regions per image. It should be noted that how Chan and Yoshida divided their data into training and testing sets is unknown. If an independent test set was not held out, their results may be biased as their systems could of been over tuned to their training data.



Feature Set	$\delta$	F-Ratio	Rank
Angular Second Moment	[0,0]	0.0655	1
	[1,0]	0.0131	23
	[2,0]	0.0134	22
	[3,0]	0.0118	24
	[4,0]	0.0163	20
	[0,1]	0.0135	21
	[1,1]	0.0241	5
	[2,1]	0.0231	7
	[3,1]	0.0182	17
	[4,1]	0.0105	25
	[0,2]	0.0187	16
	[1,2]	0.0208	14
	[2,2]	0.0292	3
	[3,2]	0.0213	13
	[4,2]	0.0230	8
	[0,3]	0.0216	12
	[1,3]	0.0226	9
	[2,3]	0.0224	10
	[3,3]	0.0258	4
	[4,3]	0.0189	15
	[0,4]	0.0174	19
	[1,4]	0.0338	2
	[2,4]	0.0177	18
	[3,4]	0.02214	11
	[4,4]	0.0233	6

Table 4.3 Fisher Ratio Values and Ranking for each ASM Feature

*4.2.3 Feature Extraction and Prediction.* The full set of 25 Laws Energy Ratios, 25 Angular Second Moment and 6 Power Spectrum Analysis features were extracted for each ROI passed by the Indexing Module with the hypothesis of containing microcalcifications. From these features, the Fisher Ratios were calculated to determine the top 6 features from each feature set as shown in Tables 4.3, 4.4, 4.5. These 6 features from each feature set were used to train a neural network for a comparison study to determine which of the texture measures give the best performance.

*4.2.4 Matching.* For each texture feature set, 5 networks with 1 to 9 hidden nodes (a total of 45 networks for each feature set) were trained using the imbalanced training set

Feature Set	Laws Mask	F-Ratio	Rank
Laws Energy Ratios	L5L5	0.3019	23
	L5S5	0.7148	2
	L5R5	0.5956	7
	L5E5	0.6207	3
	L5W5	0.6118	4
	S5L5	0.5600	9
	S5S5	0.7348	1
	S5R5	0.4574	15
	S5E5	0.5858	8
	S5W5	0.5375	10
	R5L5	0.4879	12
	R5S5	0.4200	17
	R5R5	0.2711	24
	R5E5	0.3332	20
	R5W5	0.3105	22
	E5L5	0.6039	5
	E5S5	0.6025	6
	E5R5	0.3860	19
	E5E5	0.1118	25
	E5W5	0.4659	14
	W5L5	0.4833	13
	W5S5	0.4996	11
	W5R5	0.3124	21
	W5E5	0.4439	16
	W5W5	0.4046	18

Table 4.4 Fisher Ratio Values and Ranking for each Laws Energy Ratio Feature Feature

Feature Set	Ring Radius	F-Ratio	Rank
Power Spectrum Analysis	R01	0.0480	4
	R12	0.0064	6
	R24	0.0238	5
	R48	0.2552	2
	R816	0.2641	1
	R1632	0.0650	3

Table 4.5 Fisher Ratio Values and Ranking for each Power Spectrum Analysis Feature

Feature Set	# Hidden Nodes	Probability of Detection	False ROI Rate
ASM	4	0.94	5.21
LER	4	0.94	2.36
PSA	7	0.94	1.64

Table 4.6 Training Data Set System Results including Matching Module

Parameter	Value
Global Threshold	0.5%
Local Threshold	2.0
Number of Clusters/ROI	$\geq 3$
L5R5 LER	$\geq 0.0083$
L5E5 LER	$\geq 0.0346$

Table 4.7 Parameter Settings Determined During System Development

modified backpropagation algorithm with a fixed learning rate of 0.1. Each network was trained until at least 90% of the training set microcalcifications were correctly identified. The results from testing on the training data are shown in Table 4.6. These results are biased since the network was trained with the same data it was tested with, naturally causing a high Probability of Detection. System evaluation with the Test, Evaluation and Normal Data sets will give a better representation of neural network performance.

#### 4.3 System Evaluation: Test Data Set

The Test Data was next processed to determine the effectiveness of the parameters found during system development, as shown in Table 4.7. Analysis of results from the test data was used to determine if the system parameters were over tuned for the Training Data Set. From this analysis, the parameters were "tweaked" to improve generalization before processing the final Evaluation Data.

*4.3.1 Focus of Attention Module.* Using the 17 Test Data images, the Focus of Attention module was able to detect all of the 20 microcalcification areas with an average of 44.65 ROIs per image. Table 4.8 breaks down the results for each image. The parameters for the global and local thresholds determined during training performed well against the Test Set by identifying 100% of the microcalcification regions in the 17 Test Set images.

Image	Number of Correct Regions	Rank	Total Number of Regions
AF092	1/1	4	90
AF094	1/1	13	74
AF102	1/1	6	24
AF119	2/2	1,2	36
AF121	1/1	1	28
AF128	3/3	2,3,4	31
AF130	1/1	12	28
AF141	1/1	1	51
AF150	1/1	2	61
AF160	1/1	35	63
AF162	1/1	30	53
AF168	1/1	2	84
AF170	1/1	5	43
AF186	1/1	10	20
AF192	1/1	14	18
AF202	1/1	1	26
AF204	1/1	4	29
<b>Total</b>	20/20	7.6 (mean)	759

Table 4.8 Results of Focus of Attention Module using Testing Data

The rankings for the regions were more spread out, ranging from 1 to 35, but with the majority in the top 15. Selecting the top 15 regions would result in a 90% Probability of Detection with an average 5.12 False Regions per Test Data Set image.

*4.3.2 Indexing Module.* After the FOA identified the initial ROIs, the Indexing module processed the ROIs using the parameters set during System Development. Using these threshold values, 17 of the 20 true ROIs in the Test Data Set were correctly hypothesized with an average false ROI rate of 4.9 ROIs per image. Analysis of the results indicated one region was lost due to having less than three individual microcalcifications identified in the ROI. The remaining two ROIs did not meet the Laws LER ratio thresholds. A FROC analysis was done to determine if a new threshold value should be set. Figure 4.5 shows the results of varying each parameter.

By lowering the L5E5 LER threshold to 0.0287, one of the missed ROIs can be detected, increasing the Probability of detection from 85% to 90% on the Test Set. The

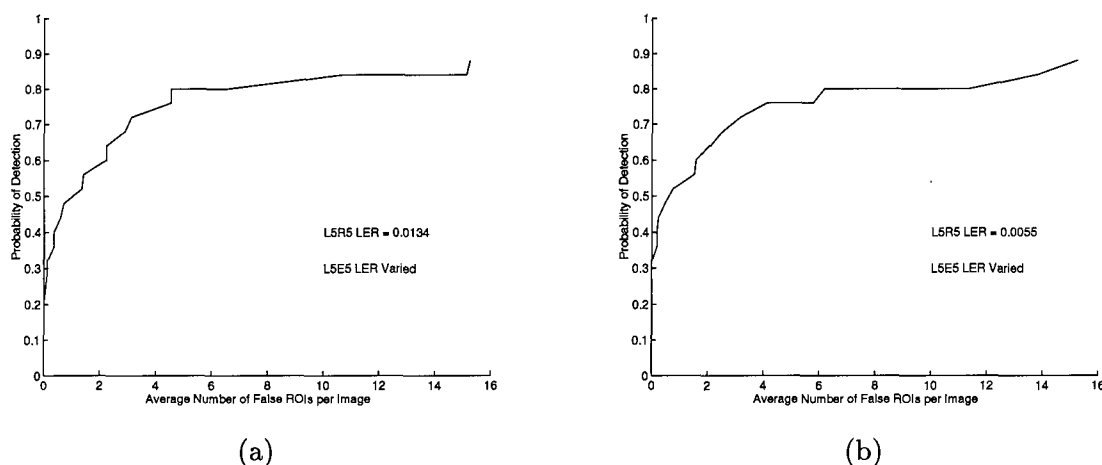


Figure 4.5 FROC Analysis of Test Data for (a) varying L5R5 LER and (b) varying L5E5 LER

False ROI Rate for the Test Data Set increased from 4.9 to 6.47 ROIs per image using the lower L5E5 LER threshold. To get the second missed ROI, both the L5R5 and L5E5 parameters had to be lowered which caused an unacceptable number of false alarms to pass through this stage. This parameter was changed before processing the Evaluation and Normal Data sets. Checking the effect of changing the parameter on the Training Data Set, the  $P_D$  remained at 100% while the False ROI Rate increased from 3.2 to 5.5 false ROIs per training set image.

**4.3.3 Matching.** The texture features were extracted for the Test Data ROIs passed by the Indexing Module. These features were evaluated with the trained networks from the system evaluation with the training data. Table 4.9 shows the performance of each feature set and the corresponding number of hidden nodes in the neural network. The Angular Second Moment Features provided little false ROI reduction while lowering Probability of Detection. The Laws Energy Ratio features cut the false ROI rate by over a factor of 2, while having the same Probability of Detection as the ASM features. The Power Spectrum Analysis features had a slightly lower Probability of Detection, but had the lowest false ROI rate.

The results from the LER and PSA features sets were analyzed to determine which regions were missed. For the LER feature set, the microcalcification regions from images

Feature Set	# Hidden Nodes	Probability of Detection	False ROI Rate
ASM	4	0.75	6.35
LER	4	0.75	2.59
PSA	7	0.70	1.82

Table 4.9 Test Data Set System Results including Matching Module

Feature Set	Feature	Saliency Value	Selected
Laws Energy Ratio	L5S5	0.4793	✓
	L5E5	0.1759	
	L5W5	0.7363	✓
	S5S5	0.3445	
	E5L5	0.2011	
	E5S5	0.9610	✓
Power Spectrum Analysis	R01	0.2188	
	R12	0.6184	✓
	R24	0.5508	✓
	R48	0.1503	
	R816	0.9892	✓
	R1632	0.3991	

Table 4.10 Ruck Saliency Values for LER and PSA Feature Sets

AF130, AF150, and AF162 were incorrectly classified. For the PSA feature set, the microcalcification regions from images AF130, AF160, AF170 and AF202 were misclassified. Notice how only one common image was missed by both feature sets. A combination of features from the LER and PSA feature sets were selected using the Ruck Saliency Metric to pick the top three features from each feature set. Table 4.10 gives the saliency values for each feature and which features were selected for use in combination. Using these features, the system Probability of Detection Rate increased to 80% and along with the False ROI Rate to 3.88 using a neural network with 2 hidden nodes. Using these features, the regions in images AF130, AF150 and AF202 were correctly classified.

#### 4.4 System Evaluation: Evaluation and Normal Data Sets

The full system with the criteria listed in Table 4.11 using the Angular Second Moment, Laws Energy Ratio, Power Spectrum Analysis and LER/PSA combination feature sets was used to evaluate the system performance using the unseen Evaluation and Normal

Parameter	Value
Global Threshold	0.5%
Local Threshold	2.0
Number of Clusters/ROI	$\geq 3$
L5R5 LER	$\geq 0.0083$
L5E5 LER	$\geq 0.0287$
Hidden Nodes	4 (ASM)
	4 (LER)
	7 (PSA)
	2 (LER/PSA)

Table 4.11 Final System Criteria Used for Evaluation/Normal Data Sets

Data Set	ASM Features		LER Features		PSA Features		LER/PSA Features	
	$P_D$	FRR	$P_D$	FRR	$P_D$	FRR	$P_D$	FRR
Evaluation	0.75	6.25	0.75	4.58	0.81	3.67	0.75	5.75
Normal	-	4.6	-	3.2	-	1.7	-	3.3

Table 4.12 System Results on Evaluation and Normal Data Sets

Data sets. Table 4.12 lists the Probability of Detection and False ROI rates for these data sets.

The Probability of Detection rate was fairly constant for all the feature sets. This reflects the system should perform at approximately this level for any data set. The False ROI Rate was slightly higher for the LER, PSA and combination feature sets. This may be caused by the images that made up the Evaluation and Normal Data sets. These images were digitized from slightly older films taken with a different X-Ray system than those used in the Training and Testing Data sets. The FOA module did correctly identify 100% of the microcalcifications in the Evaluation Data set, but the hypothesis from the Indexing Module was incorrect for 2 regions out of the 14 radiologist identified microcalcification clusters. These results validate the system FOA thresholds were not over tuned to the Training and Test Data. The Matching Module incorrectly identified the remaining 1 or 2 regions for each feature set.

The system had approximately the same False ROI Rate on the Normal Data set as with the data sets containing microcalcifications. Analysis of the results showed that the majority of the false detections were from images AF263 and AF273. It was unknown

Image Number	Number of Indexed Regions	Final Number of False ROIs Reported
214	3	2
229	5	2.5
236	4	1.5
244	1	0.5
246	2	0.5
247	3	1
263	15	9
273	15	11
275	1	0.5
286	6	3.5
<b>Total</b>	<b>55</b>	<b>3.2</b>

Table 4.13 Average Number of False Regions per Image Reported in Normal Data Set for the Four Feature Sets

why these two images accounted for the majority of false detections. Table 4.13 shows the number of False ROIs passed by the Indexing stage and the average number of false ROIs per image reported by the system for the four different feature sets.

#### 4.5 Summary

The Model Based Vision Microcalcification Detection System was developed and evaluated using 53 images with a total of 54 microcalcification regions. Three different texture measure features were examined and Fisher Ratio analysis was applied to select the features to be used in a neural network classifier. The best overall performance from the individual feature sets using the Training, Testing, Evaluation and Normal data sets was achieved with the Power Spectrum Analysis features resulting in an 83% Probability of Detection with a False ROI Rate of 2.17 regions per image. This is a comparable result to the published capabilities of approximately 83-85%  $P_D$  with 2-5 False Regions per image[13, 42]. The Power Spectrum Analysis features performed slightly better than the Laws Energy Ratio features in terms of False ROI Rate. Both had the same  $P_D$  of 83%. Table 4.14 breaks out the performance of the system for each data and feature set. These two feature sets gave better results than the Angular Second Moment features which have been used in other research[17, 9]. By creating a combination feature set based on Ruck



Data Set	ASM Features		LER Features		PSA Features		LER/PSA Features	
	$P_D$	FRR	$P_D$	FRR	$P_D$	FRR	$P_D$	FRR
Training	0.94	5.21	0.94	2.36	0.94	1.64	1.00	3.07
Testing	0.75	6.35	0.75	2.59	0.70	1.82	0.80	3.88
Evaluation	0.75	6.25	0.75	4.58	0.81	3.67	0.75	5.75
Normal	-	4.6	-	3.2	-	1.7	-	3.3
<b>Overall</b>	0.81	5.6	0.83	3.09	0.83	2.17	0.85	4.0

Table 4.14 Overall System Results for Each Data and Feature Set

Saliency of the LER and PSA feature sets, an overall  $P_D$  of 85% with a False ROI Rate of 4.0 was achieved.

## *V. Conclusions*

### *5.1 Introduction*

This chapter provides a summary of the research accomplished. The goal of this thesis was to develop a Model Based Vision system capable of identifying regions of microcalcifications in a digitized mammogram. The system identifies regions which contain microcalcifications, but does not classify them as malignant or benign. A number of unique developments in the area of feature extraction and classification were presented.

### *5.2 Summary of Methodology*

Following a Model Based Vision paradigm for computerized detection, the system was composed of 5 separate modules. The first module, Focus of Attention, used a three step process in identifying potential regions of interest (ROI). The digitized mammogram was first subjected to a non-linear remapping of the gray levels to improve the contrast and dynamic range of the microcalcifications. This image was then filtered with a Hit/Miss filtering combination. The third and final step in the FOA module was a combination of global and local thresholding to remove the areas not corresponding to microcalcifications. The FOA module was modeled after work performed by Chan[27]. Implementing the Hit/Miss/Thresholding technique on a new database confirms the potential of this method for segmenting microcalcifications. Augmenting Chan's method with the non-linear pre-processing allowed the thresholds to be set higher, reducing the number of false regions from being segmented. The FOA module correctly segmented 100% of the microcalcification regions while eliminating over 90% of the image from further processing.

The ROIs identified by the FOA module were assigned an initial hypothesis generated by the Indexing Module. This hypothesis was a function of the number of individual calcifications identified in the ROI and a novel texture energy measure called the Laws Energy Ratio. The Laws Energy Ratio compared the amount of energy in the pixels identified as part of a microcalcification in the ROI to the overall energy of the ROI which has been filtered with the Laws masks L5E5 and L5R5. The Indexing Module correctly

indexed 93% of the microcalcification regions with an average False ROI Rate of 7.55 regions per image over 53 images.

The ROIs assigned an initial hypothesis of being a region of microcalcifications had a number of features extracted based on three different texture measures: Angular Second Moment, Laws Energy Ratios and Power Spectrum Analysis. The Prediction Module used Fisher Ratio analysis to determine the top 6 features from each feature set obtained by the Feature Extraction Module. These features were then set to the final Matching Module.

The Matching module implemented a Multilayer Perceptron Neural Network trained using a modified backpropagation algorithm to classify the ROIs as normal or microcalcification tissue. A novel application of qualitatively selecting the best feature subset for microcalcification identification was accomplished. Ruck Saliency metrics were applied to identify the most relevant features in the LER and PSA feature sets to create a combined feature set resulting in an increased Probability of Detection.

### *5.3 Summary of Results*

In the first documented comparative study of texture measures for microcalcification detection on a single database, Power Spectrum Analysis features had the best overall performance, identifying 83% of the microcalcification regions with an average 2.17 false regions per image. These results were verified using an independent Evaluation Data Set to confirm the system was not biased to the Training Data. This is comparable to other research which has obtained an 85% detection rate with 2 false regions per image[27] and 83% with 5 false regions per image[42]. A combination of LER and PSA features based on Ruck Saliency metrics were selected in an attempt to improve the classification accuracy. The combination of features resulted in an overall correct classification rate of 85% with 4 false regions per image.

Although the system was not designed to classify the microcalcification regions as malignant or benign, it is interesting to note that 89% of the malignant microcalcification regions were correctly identified using the combination of PSA and LER features. This reflects the system being more sensitive to the cancerous regions. A logical extension to this

research would be to have an additional stage to classify the identified microcalcification regions as malignant or benign.

#### *5.4 Conclusion*

This research explored the application of Model Based Vision to the detection of microcalcifications. A number of novel techniques were explored for this research:

- The Hit/Miss filtering technique was effective in increasing the signal to noise ratio of the microcalcifications sufficiently such that a global and local thresholding combination could accurately segment those regions. Preprocessing the image improved performance. Frequency analysis of the Hit/Miss filtering technique showed consistent results with other research in wavelet based detection[21, 42].
- A novel texture feature, the Laws Energy Ratio, was effective in separating normal and abnormal tissue regions in the Indexing Module, correctly indexing 93% of the microcalcification regions. Using the new features for classifying the region as normal or microcalcification tissue yielded competitive results of 83% Probability of Detection with an average 3.09 False ROIs per image on 53 images.
- In the first documented, direct comparative study of three different texture measures for the classification of normal and microcalcification tissue, the Power Spectrum Analysis feature set had the best overall performance with an 83% Probability of Detection with an average 2.17 False ROIs per image.
- A neural network, trained with a modified backpropagation algorithm using a combination feature set derived from a quantitative feature selection method was able to increase the Probability of Detection, correctly identify 85% of the radiologist identified microcalcifications with an average of 4 False ROIs per image.

This research successfully met the objective of developing a complete, end to end Microcalcification Detection System as stated in Chapter I. The system was developed and evaluated using independent data sets. The final performance of the system should be a reasonable indication of system performance on any novel data set.

### *Appendix A. Database Information*

The following tables list the images used for each data set. The locations given are the center [row,column] locations of the microcalcification regions for a 2048 by 1024 image.

IMAGE	DIAGNOSIS	REGIONS	LOCATIONS
AF005	Malignant	2	[976,826],[504,665]
AF006	Malignant	3	[1194,319],[1165,363],[956,208]
AF007	Malignant	2	[603,533],[477,533]
AF008	Malignant	1	[943,416]
AF009	Malignant	1	[1410,453]
AF020	Malignant	1	[709,199]
AF022	Benign	1	[734,524]
AF024	Benign	1	[1082,654]
AF033	Malignant	1	[462,717]
AF038	Benign	1	[1154,345]
AF040	Benign	1	[1298,317]
AF045	Benign	1	[841,344]
AF047	Benign	1	[1548,607]
AF055	Malignant	1	[1313,824]

Table A.1 Training Data Set Information

IMAGE	DIAGNOSIS	REGIONS	LOCATIONS
AF092	Benign	1	[1274,747]
AF092	Benign	1	[1514,576]
AF102	Malignant	1	[579,410]
AF119	Benign	2	[865,656],[763,675]
AF121	Benign	1	[895,448]
AF128	Malignant	3	[662,474],[698,457],[758,482]
AF130	Benign	1	[1097,372]
AF141	Benign	1	[592,588]
AF150	Benign	1	[322,71]
AF160	Malignant	1	[960,789]
AF162	Malignant	1	[1263,690]
AF168	Benign	1	[925,257]
AF170	Benign	1	[851,611]
AF186	Benign	1	[1379,117]
AF192	Malignant	1	[1033,761]
AF202	Benign	1	[1124,282]
AF204	Benign	1	[1209,318]

Table A.2 Testing Data Set Information

IMAGE	DIAGNOSIS	REGIONS	LOCATIONS
AF224	Malignant	2	[1453,303],[1391,339]
AF226	Malignant	1	[1325,586]
AF240	Malignant	1	[1107,90]
AF241	Malignant	2	[236,936][364,1064]
AF259	Benign	1	[1410,453]
AF261	Benign	1	[1650,840]
AF264	Benign	1	[1621,239]
AF266	Benign	1	[1240,167]
AF267	Malignant	2	[778,552],[726,574]
AF269	Malignant	1	[1356,290]
AF282	Benign	1	[707,159]
AF284	Benign	2	[1156,114],[1184,162]

Table A.3 Evaluation Data Set Information

IMAGE	DIAGNOSIS	REGIONS	LOCATIONS
AF214	Normal	-	-
AF229	Normal	-	-
AF236	Normal	-	-
AF244	Normal	-	-
AF246	Normal	-	-
AF247	Normal	-	-
AF263	Normal	-	-
AF273	Normal	-	-
AF275	Normal	-	-
AF286	Normal	-	-

Table A.4 Normal Data Set Information

## Appendix B. Computer Code

The following sections contain the computer code used during this research. Coding was accomplished using multiple image processing environments including MATLAB and programming directly in C.

### B.1 MATLAB Code

The following M-files were used in the MATLAB environment. All main M-files and any function calls are included for completeness. Each M-file will be separated by two rows of % symbols.

```
%%%%%%%%%%%%%%%%%%%%%%%%%%%%%%%%%%%%%%%%%%%%%%%%%%%%%%%%%%%%%%%%%%%%%%%%
%This program will take the input image file name, use the defined
%parameters and perform the
%hit/miss filtering operation and the local thresholding operation.
%The surviving rois are tested for number and size of possible
%microcalcifications. A binary mask and the x,y coordinates will
%be returned to the main program.
%
%
%FUNCTIONS CALLED DURING micro_det_sys.m:
%
%local_thres: C-program for local thresholding
%  histo: MEX file for finding a histogram of a gray level image
%  main_seg: M-file for finding minimum number of rois
%  raw2viff: Khoros routine to convert file to viff type file
%  vpebble: Khoros routine to find non-connected pixel groups
% and remove groups larger than or smaller than a
% specified number
%  cluster: M-file to find number of non-connected pixel groups
%  find_asm: M-file to extract angular second moment features
%  find_ring: M-file to extract power spectrum features
%
%
%%%%%%%%%%%%%%%%%%%%%%%%%%%%%%%%%%%%%%%%%%%%%%%%%%%%%%%%%%%%%%%%%%%%%%%%
function [asm_good,asm_bad,ler_good,ler_bad,psa_good,psa_bad,combo_good,
        combo_bad,keep,toss]=micro_det_sys(file);

%define parameters
ws=64;
gthres=0.5;
lthres=2.0;
lws=51;
min_num_clusters=3;
min_LR_LER=0.00829;
```



```

min_LE_LER=0.0287;

%load mammo

mamopath='/home/pinna1/bdata/wpafbh/';
filename=[mamopath file];

if str2num(file(3:5))<=204

%Training and Testing Data Sets open using 1024 by 2048 size

fid=fopen(filename,'r');
X=fread(fid,[2048 1024],'ushort');
fclose(fid);

%remove tags from selected images

if sum(file=='af007')==5
X(1:600,1:150)=zeros(size(X(1:600,1:150)));

elseif sum(file=='af005')==5
X(1:200,1:400)=zeros(size(X(1:200,1:400)));

elseif sum(file=='af006')==5
X(1:100,480:1024)=zeros(size(X(1:100,480:1024)));

elseif sum(file=='af008')==5
X(100:600,800:1024)=zeros(size(X(100:600,800:1024)));

elseif sum(file=='af020')==5
X(1:400,750:1024)=zeros(size(X(1:400,750:1024)));

elseif sum(file=='af022')==5
X(1:200,500:1024)=zeros(size(X(1:200,500:1024)));

elseif sum(file=='af024')==5
X(1:400,800:1024)=zeros(size(X(1:400,800:1024)));

elseif sum(file=='af038')==5
X(50:300,750:1024)=zeros(size(X(50:300,750:1024)));

elseif sum(file=='af092')==5
X(1:150,700:1024)=zeros(size(X(1:150,700:1024)));

```

```

elseif sum(file=='af121')==5
X(100:225,300:425)=zeros(size(X(100:225,300:425)));

else
X=X;
end;

else;

%Evaluation and Normal Data Sets open using 1124 by 2048 size

fid=fopen(filename,'r');
X=fread(fid,[2048 1124],'ushort');
fclose(fid);

%remove tags from selected images and crop images

if sum(file=='af224')==5
X(100:400,700:1124)=zeros(size(X(100:400,700:1124)));
X=X(:,1:1024);

elseif sum(file=='af240')==5
X(1:100,500:1124)=zeros(size(X(1:100,500:1124)));
X=X(:,1:1024);

elseif sum(file=='af259')==5
X(1:200,1:700)=zeros(size(X(1:200,1:700)));
X=X(:,101:1124);

elseif sum(file=='af284')==5
X(200:600,900:1124)=zeros(size(X(200:600,900:1124)));
X=X(:,1:1024);

elseif (sum(file=='af226')==5 | sum(file=='af241')==5 |
sum(file=='af261')==5 | sum(file=='af267')==5 |
sum(file=='af269')==5)
X=X(:,101:1124);

elseif sum(file=='af214')==5
X(1:250,550:1000)=zeros(size(X(1:250,550:1000)));
X=X(:,1:1024);

elseif sum(file=='af273')==5
X(1:100,1:600)=zeros(size(X(1:100,1:600)));
X=X(:,101:1124);

```

```

elseif sum(file=='af286')==5
X(1:200,800:1124)=zeros(size(X(1:200,800:1124)));
X=X(:,1:1024);

elseif (sum(file=='af247')==5 | sum(file=='af263')==5 |
        sum(file=='af275')==5 )
X=X(:,101:1124);

else
X=X(:,1:1024);
end;
end;

%write out for local thresholding USE ONLY THE ORIGINAL IMAGE

fid=fopen('local_thres_img','wb');
fwrite(fid,X,'ushort');
fclose(fid);

param=[lthres lws];

fid=fopen('local_param','wb');
fwrite(fid,param,'float');
fclose(fid);

%%FOCUS OF ATTENTION

%Call local thresholding program

!local_thres;

%perform the sigmoid adjustment

B = .003;
x0 = 3100;
Y = 4000./(1 + exp(-B*(X - x0)));
Y = .05*X + Y;
Y=round(Y);

clear X B x0;

%perform hit/miss filtering/thresholding

```

```

load hmtfilter;

hm=conv2(Y,hmtfilter,'same');

clear Y hmtfilter param lthres lws sig;

offset=min(min(hm));
hm=hm-offset;

clear offset;

%find top pixels to keep %%

high = max(max(hm));
low = min(min(hm));
[num_pix,gl] = histo(hm,high,low,1);

total=sum(num_pix);
limit=total*(1-gthres/100);
sum_pix=0;

for gt_level=1:4096;
sum_pix=sum_pix + num_pix(gt_level);

if sum_pix>=limit;
break;
end;
end;

hmtmask=hm>=gt_level;

clear gt_level sum_pix num_pix total limit high low gl hm;

%load local thresholding mask

fid=fopen('local_mask','r');
ltmask=fread(fid,[2048 1024],'float');
fclose(fid);

%logically AND the hmtmask and ltmask

IMG=hmtmask&ltmask;
clear ltmask;

%write out hmtmask for pixel reduction by Khoros

```

```

fid=fopen('hmtmask','wb');
fwrite(fid,hmtmask,'uint1');
fclose(fid);
clear hmtmask;

!raw2viff -i hmtmask -o vfile1 -r 1024 -c 2048 -t bit
!vpbbble -i vfile1 -o hmtmaskr -val 1 -min 4 -max 45

IMG=IMG';
roi_size=ws;

main_seg;

clear IMG;

%read in reduced mask with clusters >3 pixels and <45 pixels

fid=fopen('hmtmaskr','r');
head=fread(fid,1024,'char');
IMG=fread(fid,[2048 1024],'uint1');
fclose(fid);

%%create the 25 laws matrices

L5=[1 4 6 4 1];    %% local average
S5=[-1 0 2 0 -1];  %% spot detector
R5=[1 -4 6 -4 1];  %% edge detector
E5=[-1 -2 0 2 1];  %% ripple detector
W5=[-1 2 0 -2 1];  %% wave detector

L5L5=L5'*L5;
L5S5=L5'*S5;
L5R5=L5'*R5;
L5E5=L5'*E5;
L5W5=L5'*W5;

S5L5=S5'*L5;
S5S5=S5'*S5;
S5R5=S5'*R5;
S5E5=S5'*E5;
S5W5=S5'*W5;

R5L5=R5'*L5;

```

R5S5=R5'\*S5;  
R5R5=R5'\*R5;  
R5E5=R5'\*E5;  
R5W5=R5'\*W5;

E5L5=E5'\*L5;  
E5S5=E5'\*S5;  
E5R5=E5'\*R5;  
E5E5=E5'\*E5;  
E5W5=E5'\*W5;

W5L5=W5'\*L5;  
W5S5=W5'\*S5;  
W5R5=W5'\*R5;  
W5E5=W5'\*E5;  
W5W5=W5'\*W5;

mask=[  
'L5L5'  
'L5S5'  
'L5R5'  
'L5E5'  
'L5W5'  
'S5L5'  
'S5S5'  
'S5R5'  
'S5E5'  
'S5W5'  
'R5L5'  
'R5S5'  
'R5R5'  
'R5E5'  
'R5W5'  
'E5L5'  
'E5S5'  
'E5R5'  
'E5E5'  
'E5W5'  
'W5L5'  
'W5S5'  
'W5R5'  
'W5E5'  
'W5W5'  
];

```

index_mask=[
'L5R5'
'L5E5'
];

%list of FOA roi center coordinates

xc=out2(:,2);
yc=out2(:,1);

xct=xc-ws/2;
xcb=xc+ws/2;
ycl=yc-ws/2;
ycr=yc+ws/2;

%open original image again

fid=fopen(filename,'r');
X=fread(fid,[2048 1024],'ushort');
fclose(fid);

%index rois and get features for surviving rois

num_rois=out1;

%start checking each roi for indexing,
% feature extraction and matching

for i=1:num_rois;

%check roi for extraction

if xc(i)>32 | yc(i)>32;

oroi=X(xct(i):xcb(i),ycl(i):ycr(i)); %original image roi
mroi=IMG(xct(i):xcb(i),ycl(i):ycr(i)); %mask image roi

else
break;%roi center too close to edge of image
end;

if sum(sum(mroi))==0;

break;%do not process rois with out a cluster
end;

```

```

%%INDEXING%%

%get cluster information

[num_cls,EN,D,cnts,csz]=cluster(mroi);

%get laws info for indexing

%make rois 64x64 for laws and fft processing

orois=oroi(1:64,1:64);
mrois=mroi(1:64,1:64);

%using ogrinal image

for j=1:size(index_mask,1);

eval(['x=conv2(orois,' index_mask(j,:) ','valid');']);
x=x.*(x>=0);
total=sum(sum(x));
region=sum(sum(x.*mrois(3:62,3:62)));
index_laws(j)=region/total;

end;

if (num_cls>=min_num_clusters & index_laws(1)>=min_LR_LER
& index_laws(2)>=min_LE_LER);

%%% POSSIBLE MICROCALCIFICATION ROI %%%%%%%%%

%%%FEATURE EXTRACTION%%%

%get laws ratios
%using ogrinal image

for j=1:size(mask,1);

eval(['x=conv2(orois,' mask(j,:) ','valid');']);
x=x.*(x>=0);
total=sum(sum(x));
region=sum(sum(x.*mrois(3:62,3:62)));
ler_feature(j)=region/total;

end;

```



```

%get asm features for [0,0] to [4,4]

asm_feature=findasm(orois,4);

%get psa features

psa_feature=findring(orois);

%single feature vector containing all features

features=[str2num(file(3:5)) xc(i) yc(i) num_cls
ler_feature asm_feature psa_feature];

%running total of all features for indexed rois

keep=[keep; str2num(file(3:5)) xc(i) yc(i) num_cls
ler_feature asm_feature psa_feature];

%%%MATCHING WITH NEURAL NETWORK%%%

%%%USING ASM FEATURES%%%
ASM=[1 features(:,30) features(:,36) features(:,42)
features(:,48) features(:,51) features(:,54)];
data=ASM;
load asmweights %% 4 middle nodes
train_data=nn_data_train;
W1=w1_4;
W2=w2_4;

ave=mean(train_data(:,2:I+1));
dev=std(train_data(:,2:I+1));

average=ones(n,1) * ave;
sigma=ones(n,1) * dev;

data(:,2:I+1)=(data(:,2:I+1)-average)./sigma;

data=data';

z1 = 1 ./ (1 + exp(-W1 * [data(2:I+1,1);1]));
z2 = 1 ./ (1 + exp(-W2 * [z1; 1]));

if z2>=0.2647
asmguess = 1;

```

```

else
asmguess = 0;
end;

if asmguess==1
asm_good=[asm_good;features(2:3)];
else
asm_bad=[asm_bad;features(2:3)];

%%%USING LER FEATURES%%%
LER=[1 features(:,6) features(:,8:9)
features(:,11) features(:,20:21)];
data=LER;
load lerweights %% 4 middle nodes
train_data=nn_data_train;
W1=w1_4;
W2=w2_4;

ave=mean(train_data(:,2:I+1));
dev=std(train_data(:,2:I+1));

average=ones(n,1) * ave;
sigma=ones(n,1) * dev;

data(:,2:I+1)=(data(:,2:I+1)-average)./sigma;

data=data';

z1 = 1 ./ (1 + exp(-W1 * [data(2:I+1,1);1]));
z2 = 1 ./ (1 + exp(-W2 * [z1; 1]));

if z2>=0.1741
lerguess = 1;
else
lerguess = 0;
end;
if lerguess==1
ler_good=[ler_good;features(2:3)];
else
ler_bad=[ler_bad;features(2:3)];

%%%USING PSA FEATURES%%%
PSA=[1 features(:,55:60)];
data=PSA;

```

```

load psaweights %% 7 middle nodes
W1=w1_7;
W2=w2_7;
train_data=nn_data_train;

ave=mean(train_data(:,2:I+1));
dev=std(train_data(:,2:I+1));

average=ones(n,1) * ave;
sigma=ones(n,1) * dev;

data(:,2:I+1)=(data(:,2:I+1)-average)./sigma;

data=data';

z1 = 1 ./ (1 + exp(-W1 * [data(2:I+1,1);1]));
z2 = 1 ./ (1 + exp(-W2 * [z1; 1]));

if z2>=0.4071
psaguess = 1;
else
psaguess = 0;
end;

if psaguess==1
psa_good=[psa_good;features(2:3)];
else
psa_bad=[psa_bad;features(2:3)];

%%%USING LER/PSA FEATURES%%%
combo=[1 features(:,6) features(:,9) features(:,21)
features(:,56:57) features(:,59)];
data=combo
load comboweights %% 2 middle nodes
W1=w1_2;
W2=w2_2;
train_data=nn_data_train;

ave=mean(train_data(:,2:I+1));
dev=std(train_data(:,2:I+1));

average=ones(n,1) * ave;
sigma=ones(n,1) * dev;

```

```

data(:,2:I+1)=(data(:,2:I+1)-average)./sigma;

data=data';

z1 = 1 ./ (1 + exp(-W1 * [data(2:I+1,1);1]));
z2 = 1 ./ (1 + exp(-W2 * [z1; 1]));

if z2>=0.2156
comboguess = 1;
else
comboguess = 0;
end;

if asmguess==1
combo_good=[combo_good;features(2:3)];
else
combo_bad=[combo_bad;features(2:3)];

%%%

else;
%%%NOT INDEXED MICROCALCIFICATION REGION%%%
%%%keep x,y coord and indexing features for error analysis

toss=[toss;str2num(file(3:5)) xc(i) yc(i)
num_cls index_laws(1) index_laws(2)];

end;
end;

%program complete

%%%%%%%%%%%%%%%%%%%%%%%%%%%%%%%%%%%%%%%%%%%%%%%%%%%%%%%%%%%%%%%%%%%%%%%%%%%%%%
%%%%%%%%%%%%%%%%%%%%%%%%%%%%%%%%%%%%%%%%%%%%%%%%%%%%%%%%%%%%%%%%%%%%%%%%%%%%%%

%%%%%%%%%%%%%%%%%%%%%%%%%%%%%%%%%%%%%%%%%%%%%%%%%%%%%%%%%%%%%%%%%%%%%%%%%%%%%%
%
% main_seg.m
%
%%%%%%%%%%%%%%%%%%%%%%%%%%%%%%%%%%%%%%%%%%%%%%%%%%%%%%%%%%%%%%%%%%%%%%%%%%%%%%

```

```
% Program main_seg.m that executes the segmentation functions for a
% 1024 by 2048 hit and miss thresholded mammogram.
% Original by Dru McCandles; Modified by Ron Dauk
```

```
% The requirements to run this program are:
%
% 1: A 1024x2048 matrix called IMG exists in memory
```

```
% The program parameters are:
%
% top_margin uncertainty edge distance from top/bottom of IMG
% size_margin uncertainty edge distance from sides of IMG
% min_energy minimum "energy" required for ROI to be
% considered relevant after first pass
% thresh minimum energy to survive the second pass
% box_row # rows in the sliding window (size in rows)
% box_col # cols in the sliding window (size in cols)
% -NOTE: the (image size - margin) / box size
% must be an integer !!!
```

```
%%%%%%%%%%%%%%%%%%%%%%%%%%%%%%%%%%%%%%%%%%%%%%%%%%%%%%%%%%%%%%%%%%%%%%%%
% Initial Threshold
%%%%%%%%%%%%%%%%%%%%%%%%%%%%%%%%%%%%%%%%%%%%%%%%%%%%%%%%%%%%%%%%%%%%%%%%
```

```
%mn = mean(IMG(:));
%sd = std(IMG(:));
hi_t = 1; % normally 7*sd;
%IMG(1:20,:) = zeros(20,2028);
%MASK = IMG > hi_t;
%IMG = IMG.*MASK;
%clear MASK
%figure(1)
%image(IMG)
```

```
%%%%%%%%%%%%%%%%%%%%%%%%%%%%%%%%%%%%%%%%%%%%%%%%%%%%%%%%%%%%%%%%%%%%%%%%
% Parameter Definitions
%%%%%%%%%%%%%%%%%%%%%%%%%%%%%%%%%%%%%%%%%%%%%%%%%%%%%%%%%%%%%%%%%%%%%%%%
```

```
top_margin = 0;
side_margin = 0;
%min_energy = 600; % usually = 600
%thresh = 1400; % usually = 1400
box_row = roi_size;
```

```

box_col = roi_size;

%%%%%%%%%%%%%%%%%%%%%%%%%%%%%%%%%%%%%%%%%%%%%%%%%%%%%%%%%%%%%%%%%%%%%%%%%%%%%%
% BEGIN PROGRAM
%%%%%%%%%%%%%%%%%%%%%%%%%%%%%%%%%%%%%%%%%%%%%%%%%%%%%%%%%%%%%%%%%%%%%%%%%%%%%%

% Compute the "Energy" matrix E

E = slider(IMG,top_margin,side_margin,box_row,box_col);

% Keep only those regions which have at least the minimum energy

min_energy = 1; % normally .7*mean(E(:));
[I,J] = find(E > min_energy);
I_mid = (I-1)*box_row+top_margin+(box_row/2);
J_mid = (J-1)*box_col+side_margin+(box_col/2);

% Perform the centroid migration

[G,EN]=SEG(IMG,I,J,top_margin,side_margin,min_energy,box_row,box_col);

thresh = 1; % normally 4*min_energy;
[I_final,J_final,E_final] = reducer(G,EN,thresh);

for i = 1:length(I_final)
if (I_final(i)<(box_row/2)|I_final(i)>(1020 - (box_row/2)))
E_final(i) = 0;
elseif (J_final(i)<(box_col/2)|J_final(i)>(2028 - (box_col/2)))
E_final(i) = 0;
end
end

F = find(E_final);
for i = 1:length(F);
I_clear(i) = I_final(F(i));
J_clear(i) = J_final(F(i));
E_clear(i) = E_final(F(i));
end

[m,out1]=size(E_clear);
[rank,index]=sort(E_clear');
rank=flipud(rank);
index=flipud(index);

out2=zeros(out1,2);

```

```

for i=1:out1;
out2(i,1)=I_clear(index(i));
out2(i,2)=J_clear(index(i));
end;

clear I_clear J_clear E_clear index rank I_final J_final
clear E_final top_margin side_margin box_row box_col hi_t F I
clear J I_mid J_mid E EN G min_energy

%%%%%%%%%%%%%%%%%%%%%%%%%%%%%%%%%%%%%%%%%%%%%%%%%%%%%%%%%%%%%%%%%%%%%%%%
%%%%%%%%%%%%%%%%%%%%%%%%%%%%%%%%%%%%%%%%%%%%%%%%%%%%%%%%%%%%%%%%%%%%%%%%

function E = slider(IMG,top_margin,side_margin,nrow,ncol);

% function E = slider(IMG,top_margin,side_margin,nrow,ncol);
%
% function that returns the matrix E of the sum of the abs of the pixel
% values in IMG, where IMG is a 1020x2028 reconstructed wavelet image
% of a mammogram. Each entry in E is the 'energy' of
% a nrow by ncol size piece of IMG, with a 1-to-1 correspondance
% between the location of E(i,j) and
% the location of the 99x100 piece of IMG for which it was computed.
%
% To determine where E(i,j) came from, find:
% row_start = (i-1)*nrow + top_margin + 1
% col_start = (j-1)*ncol + side_margin + 1
%
% The roi is located at
% (row_start:row_start+nrow-1,col_start:col_start+ncol-1)
%
% The energy is computed by sliding a non-overlapping
% nrowxncol box over IMG

[nr,nc] = size(IMG); % This should be 1020 x 2028 !!
rboxes = (nr - 2*top_margin)/nrow;
cboxes = (nc - 2*side_margin)/ncol;

for x = 1:cboxes
for y = 1:rboxes
row_index = top_margin + ((y-1)*nrow) + 1;
col_index = side_margin + ((x-1)*ncol) + 1;
ROI = IMG(row_index:(row_index+nrow-1),col_index:(col_index+ncol-1));
E(y,x) = sum(sum(abs(ROI)));
end

```

end

%%  
%%

function [G,EN]=SEG(IMG,I,J,top\_margin,side\_margin,min\_energy,srow,scol);

%function [G,EN]=SEG(IMG,I,J,top\_margin,side\_margin,min\_energy,srow,scol);

tol = 3;

[Sr,Sc] = size(IMG);

L = length(I);

for i = 1:L

i;

row\_index = top\_margin + ((I(i)-1)\*srow) + 1;

col\_index = side\_margin + ((J(i)-1)\*scol) + 1;

ROI=IMG(row\_index:(row\_index+srow-1),col\_index:(col\_index+scol-1));

C = centroid(abs(ROI));

% recompute the new ROI

nri = C(1) + row\_index - (srow/2) + 1;

if nri < (top\_margin + 1)

nri = top\_margin + 1;

end

nrif = C(1) + row\_index + (srow/2);

if nrif > (Sr - top\_margin)

nrif = Sr - top\_margin;

end

nci = C(2) + col\_index - (scol/2) + 1;

if nci < (side\_margin + 1)

nci = side\_margin + 1;

end

ncif = C(2) + col\_index + (scol/2);

if ncif > (Sc - side\_margin)

ncif = (Sc - side\_margin);

end

ROI = IMG(nri:nrif,nci:ncif);

OCX = [C(1)+row\_index C(2)+col\_index];

row\_index = nri;

col\_index = nci;

C = centroid(abs(ROI));



```

NCX = [C(1)+nri C(2)+nci];
d = sqrt((OCX - NCX)*(OCX - NCX)');
EN(i) = sum(sum(abs(ROI)));
n = 1;
while d > tol
nri = C(1) + row_index - (srow/2) + 1;
if nri < (top_margin + 1)
nri = top_margin + 1;
end
nrif = C(1) + row_index + (srow/2);
if nrif > (Sr - top_margin)
nrif = Sr - top_margin;
end
nci = C(2) + col_index - (scol/2) + 1;
if nci < (side_margin + 1)
nci = side_margin + 1;
end
ncif = C(2) + col_index + (scol/2);
if ncif > (Sc - side_margin)
ncif = (Sc - side_margin);
end
ROI = IMG(nri:nrif,nci:ncif);
EN(i) = sum(sum(abs(ROI)));
if EN(i) < min_energy
d = 0;
end
OCX = [C(1)+row_index C(2)+col_index];
row_index = nri;
col_index = nci;
C = centroid(abs(ROI));
NCX = [C(1)+nri C(2)+nci];
d = sqrt((OCX - NCX)*(OCX - NCX)');
n = n + 1;
end
new_I(i) = C(1) + nri;
new_J(i) = C(2) + nci;
end
G = [new_I' new_J'];

%%%%%%%%%%%%%%%%%%%%%%%%%%%%%%%%%%%%%%%%%%%%%%%%%%%%%%%%%%%%%%%%%%%%%%%%
%%%%%%%%%%%%%%%%%%%%%%%%%%%%%%%%%%%%%%%%%%%%%%%%%%%%%%%%%%%%%%%%%%%%%%%%

function [I_final,J_final,E_final] = reducer(G,EN,thresh)

% program reducer.m that removes duplicate rois

```

```

%(i.e., rois that have centers that are within 20 pixels of each other)
% - it keeps the roi with the highest energy.

```

```

% The row,col components are in a L by 2 matrix G, and the Energy is in
% a L by 1 vector EN

```

```

L = length(EN);
wun = ones(L,1);

```

```

for i = 1:L
    tmp = wun*G(i,:);
    A = G - tmp;
    D = sqrt(diag(A*A'));
    DIST = [DIST D];
    DIST(i,i) = 1000;
end

```

```

[II,JJ] = find(DIST < 30);
for i = 1:length(II);
    if EN(II(i)) > EN(JJ(i))
        EN(JJ(i)) = 0;
    else
        EN(II(i)) = 0;
    end
end

```

```

for i = 1:L
    if EN(i) > 99999500 % usually 9500
        EN(i) = 0;
    end
end

```

```

F = find(EN > thresh);
for i = 1:length(F);
    I_final(i) = G(F(i),1);
    J_final(i) = G(F(i),2);
    E_final(i) = EN(F(i));
end

```

```

%%%%%%%%%%%%%%%%%%%%%%%%%%%%%%%%%%%%%%%%%%%%%%%%%%%%%%%%%%%%%%%%%%%%%%%%
%%%%%%%%%%%%%%%%%%%%%%%%%%%%%%%%%%%%%%%%%%%%%%%%%%%%%%%%%%%%%%%%%%%%%%%%

```

```

function C = centroid(ROI);

```

```
% function C = centroid(ROI);
%
% This function computes a weighted centroid C = [rc cc] of the matrix ROI
%
```

```
[I,J,V] = find(ROI);
S = sum(V);
rc = sum(I.*V)/S;
cc = sum(J.*V)/S;
C = [round(rc) round(cc)];
```

```
%%%%%%%%%%%%%%%%%%%%%%%%%%%%%%%%%%%%%%%%%%%%%%%%%%%%%%%%%%%%%%%%%%%%%%%%
%%%%%%%%%%%%%%%%%%%%%%%%%%%%%%%%%%%%%%%%%%%%%%%%%%%%%%%%%%%%%%%%%%%%%%%%
```

```
function [num,E,D,M,csize] = cluster(IMG);
```

```
% function [num,E,D,M,csize] = cluster(IMG);
%
% This function takes in an image IMG and determines the number of unique
% clusters (num), the abs energy of each cluster (E), the distance of the
% center of each cluster from the centroid (D), and the center coordinate
% of each cluster (M).
%
% The function works using a two-pass loop: The first pass groups all
% pixels that are left-right of each other together first, and then
% top-bottom second by assigning each pixel a cluster number C(i).
% The second pass then groups all of the 'sub-clusters' together that
% are top-bottom connected by reassigning all the cluster numbers from one
% to match the other.
```

```
[I,J,V] = find(abs(IMG));
l = length(I);
```

```
% first pass - assign same row clusters
```

```
C(1) = 1;
cmax = 1;
cind = cmax;
for i = 2:l
new_col = J(i) - J(i-1);
if new_col == 0
t = find((I == I(i)) & (J == (J(i) - 1)));
if t == []
if I(i) == (I(i-1) + 1)
```

```

C(i) = cind;
else
cmax = cmax + 1;
cind = cmax;
C(i) = cind;
end
else
cind = C(t);
C(i) = cind;
end
elseif new_col == 1
t = find((I == I(i)) & (J == (J(i) - 1)));
if t == []
cmax = cmax + 1;
cind = cmax;
C(i) = cind;
else
cind = C(t);
C(i) = cind;
end
else
cmax = cmax + 1;
cind = cmax;
C(i) = cind;
end
end

% second pass - assign same column clusters

for i = 2:l
if (J(i) == J(i-1)) & (I(i) == I(i-1)+1)
if C(i) ~= C(i-1)
t = C(i-1);
T = find(C == t);
q = length(T);
for k = 1:q
C(T(k)) = C(i);
end
end
end
end

CENT = centroid(IMG);

% determine the number of unique clusters, size, energy & distance

```

```

num = 0;
for i = 1:cmax
T = find(C == i);
if T ~= []
num = num + 1;
s = length(T);
csize(num) = s;
e = 0;
rowsum = 0;
colsum = 0;
for k = 1:s
e = e + V(T(k));
rowsum = rowsum + V(T(k))*I(T(k));
colsum = colsum + V(T(k))*J(T(k));
end
E(num) = e;
rowm = rowsum/e;
colm = colsum/e;
Mn = [rowm colm];
M(num,1:2) = Mn;
D(num) = sqrt((Mn - CENT)*(Mn - CENT)');
end
end

```

```

%%%%%%%%%%%%%%%%%%%%%%%%%%%%%%%%%%%%%%%%%%%%%%%%%%%%%%%%%%%%%%%%%%%%%%%%
%%%%%%%%%%%%%%%%%%%%%%%%%%%%%%%%%%%%%%%%%%%%%%%%%%%%%%%%%%%%%%%%%%%%%%%%

```

```

%single hidden layer, sigmoid activation function, single output
%neural net
%      TRAINING IN BATCH MODE
%[err_c0,err_c1,W1,W2]=seltrn(data,HL,maxepochs,lr,clamp,type);
%
%INPUT:
%
%data:  1st col class, remaining cols features, # of row=# of samples
%      HL:  number of desired hidden nodes
%maxepochs:  maximum number of epochs to train
% lr:  learning rate
%      clamp:  clamp output > 1-clamp to 1-clamp or <clamp to clamp
%      type:  select backprop method: 0 normal, 1 imbalanced
%
%OUTPUT:
%   err_c0:  error for class 0 for each epoch
%   err_c1:  error for class 1 for each epoch

```

```

% W1: final weights for input to hidden layer
% W2: final weights for hidden layer to output node
%
%This program will train a neural net for an imbalanced training set
%with two classes with a selectable number of hidden nodes and a
%single output node.

function

[err_c0,err_c1,W1,W2,dzdx]=seltrn(data,HL,maxepochs,lr,clamp,type)

%%rand seed value

rand('seed',sum(100*clock));
[n,I]=size(data);
I=I-1;

%normalize data

ave=mean(data(:,2:I+1));
dev=std(data(:,2:I+1));

average=ones(n,1) * ave;
sigma=ones(n,1) * dev;

data(:,2:I+1)=(data(:,2:I+1)-average)./sigma;

data=data';

%initialize weights in the net

W1=rand(HL,I+1)-0.5;  %[HL by I+1]
W2=rand(1,HL+1)-0.5; %[1 by HL+1]

err_c0=[];
err_c1=[];
epoch=0;

while epoch<maxepochs

%Initialize variables
mse0=[];
mse1=[];
index=randperm(n);
count0=1;

```

```

count1=1;
z1_c0=[];
z1_c1=[];
z2_c0=[];
z2_c1=[];
X_c0=[];
X_c1=[];
n0=0;
n1=0;

for i=1:n;

%desired output
d(i)=data(1,index(i));

%feature vector with bias(I+1 by n)
X(:,i)=[data(2:I+1,index(i)); 1];

%compute activation fuctions

%hidden layer (HL by n)
z1(:,i)=1./(1+exp(-W1 * X(:,i)));

%output layer (1 by n)
z2(1,i)=1./(1+exp(-W2 * [z1(:,i);1]));

%clamp output values

if z2(1,i)>(1-clamp);

z2(1,i)=1-clamp;

elseif z2(1,i)<clamp;

z2(1,i)=clamp;

else;

z2(1,i)=z2(1,i);

end;

%divide input, hidden and output layer results by class

```

```

    if d(i)==1;
    X_c1=[X_c1 X(:,i)];
    z1_c1=[z1_c1 z1(:,i)];
    z2_c1=[z2_c1 z2(1,i)];
    n1=n1+1;
    else;
    X_c0=[X_c0 X(:,i)];
    z1_c0=[z1_c0 z1(:,i)];
    z2_c0=[z2_c0 z2(1,i)];
    n0=n0+1;
    end;

end; %%all train samples through the net

%%find first derivative of hidden and output layers

%derivative of hidden layer(HL by n0)
dz1_c0=z1_c0.*(1-z1_c0);

%derivative of output layer (1 by n0)
dz2_c0=z2_c0.*(1-z2_c0);

%derivative of hidden layer(HL by n1)
dz1_c1=z1_c1.*(1-z1_c1);

%derivative of output layer(1 by n1)
dz2_c1=z2_c1.*(1-z2_c1);

dout_c0=dz2_c0 .* (clamp-z2_c0); %(1 by n0)
temp_c0=W2' * dout_c0; %(HL+1 by n0)
dhl_c0 = dz1_c0 .* temp_c0(1:HL,:); %(HL by n0)

dout_c1=dz2_c1 .* (1-clamp-z2_c1); %(1 by n1)
temp_c1=W2' * dout_c1; %(HL+1 by n1)
dhl_c1 = dz1_c1 .* temp_c1(1:HL,:); %(HL by n1)

%calculate gradients for each class

GE_W1_c0=dhl_c0 * X_c0';
GE_W2_c0=dout_c0 * [z1_c0;ones(1,n0)]';

GE_W1_c1=dhl_c1 * X_c1';

```



```

GE_W2_c1=dout_c1 * [z1_c1;ones(1,n1)]';

%update the weights

if type==0;

%regular backprop GE=GE_c0 + GE_c1

W1 = W1 + lr*(GE_W1_c0 + GE_W1_c1);  %(HL by I+1)
W2 = W2 + lr*(GE_W2_c0 + GE_W2_c1);  %(1 by HL+1)

else;

%imbalanced training set

%find unit vectors for each gradient

unit_GE_W1_c0=GE_W1_c0/sqrt(sum(sum(GE_W1_c0.^2)));
unit_GE_W1_c1=GE_W1_c1/sqrt(sum(sum(GE_W1_c1.^2)));
unit_GE_W2_c0=GE_W2_c0/sqrt(sum(GE_W2_c0.^2));
unit_GE_W2_c1=GE_W2_c1/sqrt(sum(GE_W2_c1.^2));

%set direction to the bisecting angle between the class GE vectors

ang_GE_W1=(unit_GE_W1_c0 + unit_GE_W1_c1)/2;
ang_GE_W2=(unit_GE_W2_c0 + unit_GE_W2_c1)/2;

%calculate magnitude of GE vectors

mag_GE_W1=sqrt(sum(sum((GE_W1_c0 + GE_W1_c1).^2)));
mag_GE_W2=sqrt(sum((GE_W2_c0 + GE_W2_c1).^2));

%create new GE vectors

GE_W1=mag_GE_W1*ang_GE_W1;
GE_W2=mag_GE_W2*ang_GE_W2;

%update weights with new backprop

W1=W1+lr*GE_W1;
W2=W2+lr*GE_W2;

end;

%calculate the mse for each class

```

```

for i=1:n
    if d(i)==0;
        mse0(count0)=(clamp-z2(i))^2;
        count0=count0+1;
    else;
        mse1(count1)=(1-clamp-z2(i))^2;
        count1=count1+1;
    end;
end;

%% compute epoch error for each class

epoch_err_c0=mean(mse0);
epoch_err_c1=mean(mse1);
err_c0=[err_c0 epoch_err_c0];
err_c1=[err_c1 epoch_err_c1];
epoch=epoch+1;

end;

% Ruck Feature Saliency

dzdx=zeros(1,I);
for i=1:n

    z1 = 1 ./ (1 + exp(-W1 * X(:,i)));
    z2 = 1 ./ (1 + exp(-W2 * [z1; 1]));
    fprime1 = z1 .* (1-z1);
    fprime2 = z2 .* (1-z2);

    %dzdx contains each feature's saliency for all training samples

    dzdx1=abs((W1(:,1:I))*(((W2(:,1:HL))*fprime2).*fprime1)))');
    dzdx=dzdx + dzdx1;

end % (for i=1:n)

dzdx=dzdx/max(dzdx);
dzdx

```

## B.2 C Code

This section contains the C code developed to accomplish the local thresholding. The program requires a 1024 by 2048, unsigned short integer data type, binary image file named "local\_thres\_img" be available in the current directory. A parameter file with the threshold and local window sizes must be in a file named "local\_param" saved as floating point data type. The program will then test every pixel in the image to determine if it is greater than the mean plus the threshold times the standard deviation of the pixels surrounding the test pixel. The size of the region is defined by the local window size parameter. The system will output a binary image with ones where the pixel met the criteria and zeros where it did not. This file is written to disk with the name "local\_mask" and saved as a floating point data type.

This code can be compiled using the following at the command line on a Unix platform. `cc -o output.exe local_thres.c -lm`

```
#include <stdio.h>
#include <math.h>
#include <stdlib.h>

#define max_rows 1024
#define max_cols 2048

float mammo[max_rows][max_cols];
float new_mask[max_rows][max_cols];
unsigned short bufin[max_rows*max_cols];
float bufout[max_rows*max_cols];
char header[1024];

main()
{
FILE *ifp,*ofp;
int nread,nitems=2,count=0,m,k;
float oldsum,oldsumofsqr,sum,sumofsquares;
float mean,std,low_t,win_size,param[2],temp;
int row,col,ws;

/* Read in Mammogram */

ifp = fopen("local_thres_img","r");
nread = fread(bufin, sizeof(unsigned short), max_rows*max_cols, ifp);
fclose(ifp);
```

```

for (row=0;row<max_rows;row++)
for (col=0;col<max_cols;col++)
mamo[row][col]= (float) bufin[row*max_cols+col];

/* Read in Values for parameters*/

ifp = fopen("local_param","r");
nread = fread(param, sizeof(float), nitems, ifp);
fclose(ifp);

low_t=param[0];
win_size=param[1];
ws = (int) win_size;

/* Fill outer edge of mask with zeros */

for (row=0;row<((ws-1)/2);row++)
for (col=0;col<max_cols;col++)
new_mask[row][col]=0.0;

for (row=max_rows-((ws-1)/2);row<max_rows;row++)
for (col=0;col<max_cols;col++)
new_mask[row][col]=0.0;

for (row=((ws-1)/2);row<max_rows-((ws-1)/2);row++)
for (col=0;col<((ws-1)/2);col++)
new_mask[row][col]=0.0;

for (row=((ws-1)/2);row<max_rows-((ws-1)/2);row++)
for (col=max_cols-((ws-1)/2);col<max_cols;col++)
new_mask[row][col]=0.0;

/* test first pixel */

sum = 0.0;
sumofsquares = 0.0;
for (row=0; row<ws; row++)
    for (col=0; col<ws; col++)
    {
sum = sum + mamo[row][col];
sumofsquares=sumofsquares+mamo[row][col]*mamo[row][col];
    }
oldsum = sum;
oldsumofsqr = sumofsquares;

```

```

    m = (ws-1)/2;
    mean = sum/(win_size*win_size);
    temp=(sumofsquares-((sum*sum)/(win_size*win_size)))/(win_size*win_size-1);
    if (temp<=1.0)
    std=temp;
    else
    std= (float) sqrt( (double) temp);

if (mamo[m][m]>mean+low_t*std && mean>1200.0)
new_mask[m][m]=1.0;
else
new_mask[m][m]=0.0;

/* test all other pixels */

for (row=m; row<max_rows-m; row++)
{
    for (col=m+1; col<max_cols-m; col++)
    {
        for (k=-m; k<m+1; k++)
        {
            sum = sum - mamo[row+k][col-m-1] + mamo[row+k][col+m];
            sumofsquares=sumofsquares-mamo[row+k][col-m-1]*mamo[row+k][col-m-1]
+ mamo[row+k][col+m]*mamo[row+k][col+m];
        }
        mean = sum/(win_size*win_size);
        temp=(sumofsquares-((sum*sum)/(win_size*win_size)))/(win_size*win_size-1);
        if (temp<=1.0)
        std=temp;
        else
        std= (float) sqrt( (double) temp);

if (mamo[row][col]>mean+low_t*std && mean>1200.0)
    new_mask[row][col]=1.0;
else
new_mask[row][col]=0.0;
    }

    sum = oldsum; /* update sum and sumofsquares */
    sumofsquares = oldsumofsqr;
    for (k=-m; k<m+1; k++)
    {
        sum = sum - mamo[row-m][m+k] + mamo[row+m+1][m+k];
        sumofsquares = sumofsquares - mamo[row-m][m+k]*mamo[row-m][m+k]

```

```

    + mammo[row+m+1][m+k]*mammo[row+m+1][m+k];
}

    oldsum = sum;                /* update oldsum and OldSumOfSqr */
    oldsumofsqr = sumofsquares;
/* calculate statdiff for 1st nonzero */
    /* output pixel in next row */

mean = sum/(win_size*win_size);
temp=(sumofsquares-((sum*sum)/(win_size*win_size)))/(win_size*win_size-1);
    if (temp<=1.0)
std=temp;
    else
    std= (float) sqrt( (double) temp);

    if (mammo[row][col]>mean+low_t*std && mean>1200.0)
new_mask[row][col]=1.0;
    else
new_mask[row][col]=0.0;
}

/* Output mask of potential regions */

for (row=0;row<max_rows;row++)
for (col=0;col<max_cols;col++)
bufout[row*max_cols+col]=new_mask[row][col];

ofp=fopen("local_mask","w");
nread=fwrite(bufout, sizeof(float),max_rows*max_cols,ofp);
fclose(ofp);
printf("mask completed, \n");
}

```

## Bibliography

1. *CA Cancer Journal*, 33:255 (1983).
2. *Cancer Facts and Figures*. Technical Report, American Cancer Society, 1991.
3. *Breast Cancer: New Perspectives Can Replace Unrealistic Fears*. Technical Report ISSN 0741-6254, Mayo Foundation for Medical Education and Research, October 1994.
4. *Model-Driven Automatic Target Recognition*. Technical Report, Wright-Patterson AFB OH: Wright Laboratory, October 1994.
5. Anand, R., et al. "An Improved Algorithm for Neural Network Classification of Imbalanced Training Sets," *IEEE Transactions on Neural Networks*, 4(6):962-969 (November 1993).
6. Brettell, D.S., et al. "Automatic Micro-calcification Localisation using Matched Fourier Filtering." *Digital Mammography*. 21-30. Amsterdam, The Netherlands: Elsevier Science B.V., 1994. 2nd International Workshop on Digital Mammography.
7. Chan, Heang-Ping, et al. "Image feature analysis and computer-aided diagnosis in digital radiography: Automated detection of microcalcifications in mammography," *Medical Physics*, 14(4):538-548 (August 1987).
8. Chan, Heang-Ping, et al. "Computer-aided Detection and Microcalcification in Mammograms: Methodology and Preliminary Clinical Study," *Investigative Radiology*, 23:664-671 (1988).
9. Chitre, Yateen, et al. "Artificial Neural Network Based Classification of Mammographic Microcalcifications Using Image Structure Features," *International Journal of Pattern Recognition and Artificial Intelligence*, 7(6):1377-1401 (1993).
10. Chitre, Yateen, et al. "Classification of mammographic microcalcifications using image structure and cluster features." *Digital Mammography*. 31-40. Amsterdam, The Netherlands: Elsevier Science B.V., 1994. 2nd International Workshop on Digital Mammography.
11. Duda, Richard O. and Peter E. Hart. *Pattern Classification and Scene Analysis*. New York: John Wiley and Sons, 1973.
12. Eisenbies, Christopher L. *Classification of Ultra High Range Resolution Radar Using Decision Boundary Analysis*. MS thesis, AFIT/GE/ENG/94D-07, Graduate School of Engineering, Air Force Institute of Technology (AETC), Wright-Patterson AFB OH, 1994.
13. Giger, Maryellen L. "Computer-aided Diagnosis," *RSNA Categorical Course in Physics*, 287-302 (1994).
14. Goodman, John W. *Statistical Optics*. New York: John Wiley and Sons, 1985.
15. Harrup, Georgia K. *ROC Analysis of IR Segmentation Techniques*. MS thesis, AFIT/GE/ENG/94D-15, Graduate School of Engineering, Air Force Institute of Technology (AETC), Wright-Patterson AFB OH, 1994.

16. Hoffmeister, Jeffery W. Personal interviews, May-Nov 1995. Aerospace Physician. AL/CFHV, Wright-Patterson AFB, OH.
17. Kocur, Catherine M., et al. "Neural Network Selection for Breast Cancer Diagnosis." Accepted to IEEE Transactions on Medicine and Biology, to appear in early 1996, 1995.
18. Kocur, Catherine Mary. *Computer-Aided Breast Cancer Diagnosis*. MS thesis, AFIT/GSO/ENS/94-D-03, Graduate School of Engineering, Air Force Institute of Technology (AETC), Wright-Patterson AFB OH, 1994.
19. Kukulich, Linda and Richard Lippmann. *LNKnet User's Guide*. MIT Lincoln Laboratory, July 1993.
20. Martin, Curtis E. *Non-Parametric Bayes Error Estimation For UHRR Target Identification*. MS thesis, AFIT/GE/ENG/93D-26, Graduate School of Engineering, Air Force Institute of Technology (AETC), Wright-Patterson AFB OH, 1993.
21. McCandles, Dru. *Detection of Clustered Microcalcifications Using Wavelets*. MS thesis, AFIT/GE/ENG/95-D-, Graduate School of Engineering, Air Force Institute of Technology (AETC), Wright-Patterson AFB OH, 1995.
22. Metz, C. E. and J. H. Shen. "Gains in accuracy from replicated readings of diagnostic images: prediction and assessment in terms of ROC analysis," *Medical Decision Making*, 12:60-75 (1992).
23. Miller, Peter and Sue Astley. "Classification of breast tissue by texture analysis," *Image and Vision Computing*, 10(5):277-281 (1992).
24. Morrow, W. M., et al. "Region-based contrast enhancement of mammograms," *IEEE Transactions on Medical Imaging*, 11(3) (September 1992).
25. Myers, Lemuel R., et al. "Image Perception and Enhancement of the Visually Impaired," *IEEE engineering in Medicine and Biology* (1995).
26. Nishikawa, Robert M., et al. "Computer-aided detection of clustered: An improved method for grouping detected signals," *Medical Physics*, 20(6):1661-1666 (Nov/Dec 1993).
27. Nishikawa, Robert M., et al. "Computer-aided detection and diagnosis of masses and clustered microcalcification from digital mammograms," *SPIE*, 1905:422-432 (November 1994).
28. Parker, J, et al. "Classification of ductal carcinoma in situ by image analysis of calcifications from digital mammograms," *The British Journal of Radiology*, 68:150-159 (February 1993).
29. Parsons, Thomas. *Voice and Speech Processing*. McGraw-Hill Book Co, 1987.
30. Pietikainen, Matti, et al. "Texture Classification Using Averages of Local Pattern Matches." *Proceedings of the 6th International Conference on Pattern Recognition*. 301-303. IEEE Computer Society Press, October 1992.
31. Rogers, Steven K. and Matthew Kabrisky. *An Introduction to Biological and Artificial Neural Networks for Pattern Recognition*. SPIE, 1991.



32. Rogers, Steven K., et al. "Artificial neural networks for early detection and diagnosis of cancer," *Cancer Letters*, 77:79-83 (1994).
33. Rogers, Steven K., et al. "Artificial Neural Networks for Automatic Object Recognition," *SPIE Institute Series on Automatic Object Recognition*, 231-243 (April 1990).
34. Ruck, Dennis W., et al. "Feature Selection Using A Multilayer Perceptron," *Journal of Neural Network Computing*, 2(2):40-48 (Oct 1990).
35. Smiley, Steven E. *Image Segmentation Using Affine Wavelets*. MS thesis, AFIT/EN/ENG/91D-50, Graduate School of Engineering, Air Force Institute of Technology (AETC), Wright-Patterson AFB OH, 1991.
36. Smith, R. A. "Epidemiology of Breast Cancer," *RSNA Categorical Course in Physics*, 21-33 (1994).
37. Sontag, E. and H. Sussmann. "Backpropagation Separates When Perceptrons Do." *Proceedings of the International Conference on Neural Networks*. 639-642. 1988.
38. Steppe, Jean M. *Feature and Model Selection in Feedforward Neural Networks*. PhD dissertation, Graduate School of Engineering, Air Force Institute of Technology (AETC), Wright-Patterson AFB OH, 1994.
39. Steppe, Jean M., et al. "Integrated Feature and Architecture Selection." submitted to IEEE Transactions on Neural Networks, 1994.
40. Tanne, Janice Hopkins. "Everything You Need to Know About Breast Cancer...But Were Afraid to Ask," *New York [GNYC]*, 26:52-62 (1993).
41. Weszka, J. S., et al. "A Comparative Study of Texture Measures for Terrain Classification," *IEEE Transactions on Systems, Man, and Cybernetics*, 6(4):269-284 (April 1976).
42. Yoshida, Hiroyuki, et al. "Automated Detection of Clustered Microcalcifications in Digital Mammograms Using Wavelet Transform Techniques," *SPIE Image Processing*, 2167:868-886 (1994).

## Vita

Captain Ronald C. Dauk [REDACTED]. He graduated from Janesville High School in 1987 and attended North Dakota State University, graduating with a Bachelor of Science in Electrical Engineering in May, 1991. Upon graduation, he received a reserve commission in the United State Air Force. He was assigned his first tour of duty at Wright Patterson AFB, Ohio. He was assigned to the Surface Strike Section, Mission Avionics Division, Avionics Directorate, Wright Laboratory where he was responsible for monitoring and evaluating developing Automatic Target Recognition (ATR) systems. He was then assigned as Program Manager for the FLIR and Automatic Target Cues Insertion into LANTIRN (FRACTIL) program which developed and evaluated three potential target recognition systems for the LANTIRN Targeting Pod. Captain Dauk entered the School of Engineering, Air Force Institute of Technology, in May 1994, to obtain his Masters of Science degree in Electrical Engineering, with concentration in Electro-Optics and Pattern Recognition.

[REDACTED]  
[REDACTED]  
VITA-1

REPORT DOCUMENTATION PAGE			Form Approved OMB No. 0704-0188	
Public reporting burden for this collection of information is estimated to average 1 hour per response, including the time for reviewing instructions, searching existing data sources, gathering and maintaining the data needed, and completing and reviewing the collection of information. Send comments regarding this burden estimate or any other aspect of this collection of information, including suggestions for reducing this burden, to Washington Headquarters Services, Directorate for Information Operations and Reports, 1215 Jefferson Davis Highway, Suite 1204, Arlington, VA 22202-4302, and to the Office of Management and Budget, Paperwork Reduction Project (0704-0188), Washington, DC 20503.				
1. AGENCY USE ONLY (Leave blank)		2. REPORT DATE December 1995		3. REPORT TYPE AND DATES COVERED Master's Thesis
4. TITLE AND SUBTITLE COMPUTER AIDED DETECTION OF MICROCALCIFICATIONS USING TEXTURE ANALYSIS			5. FUNDING NUMBERS	
6. AUTHOR(S) Ronald C. Dauk Captain, USAF				
7. PERFORMING ORGANIZATION NAME(S) AND ADDRESS(ES) Air Force Institute of Technology, WPAFB OH 45433-6583			8. PERFORMING ORGANIZATION REPORT NUMBER AFIT/GEO/ENG/95D-01	
9. SPONSORING / MONITORING AGENCY NAME(S) AND ADDRESS(ES)			10. SPONSORING / MONITORING AGENCY REPORT NUMBER	
11. SUPPLEMENTARY NOTES				
12a. DISTRIBUTION / AVAILABILITY STATEMENT Approved for public release; Distribution Unlimited			12b. DISTRIBUTION CODE  A	
13. ABSTRACT (Maximum 200 words) A comparative study of texture measures for the classification of breast tissue is presented. The texture features investigated include Angular Second Moments, Power Spectrum Analysis and a novel feature, Laws Energy Ratios. The texture study was accomplished as part of the development of a Model Based Vision (MBV) system for the automatic detection of microcalcifications. An overview of the Microcalcification Detection System is presented, which applies image differencing techniques, feature selection methods, and neural networks for locating microcalcification clusters in mammograms. The Power Spectrum Analysis feature set had the best overall performance with an 83% Probability of Detection and an average False ROI Rate of 2.17 ROIs per image over 53 mammograms. A combination of Laws Energy Ratio and Power Spectrum Analysis features selected using Ruck Saliency metrics achieved an increased Probability of Detection of 85% with an average 4 false ROIs per image.				
14. SUBJECT TERMS Breast Cancer, Microcalcifications, Image Differencing, Image Texture Measures, Neural Networks, Feature Selection			15. NUMBER OF PAGES 106	
			16. PRICE CODE	
17. SECURITY CLASSIFICATION OF REPORT UNCLASSIFIED	18. SECURITY CLASSIFICATION OF THIS PAGE UNCLASSIFIED	19. SECURITY CLASSIFICATION OF ABSTRACT UNCLASSIFIED	20. LIMITATION OF ABSTRACT UL	

## GENERAL INSTRUCTIONS FOR COMPLETING SF 298

The Report Documentation Page (RDP) is used in announcing and cataloging reports. It is important that this information be consistent with the rest of the report, particularly the cover and title page. Instructions for filling in each block of the form follow. It is important to *stay within the lines* to meet *optical scanning requirements*.

**Block 1. Agency Use Only (Leave blank).**

**Block 2. Report Date.** Full publication date including day, month, and year, if available (e.g. 1 Jan 88). Must cite at least the year.

**Block 3. Type of Report and Dates Covered.** State whether report is interim, final, etc. If applicable, enter inclusive report dates (e.g. 10 Jun 87 - 30 Jun 88).

**Block 4. Title and Subtitle.** A title is taken from the part of the report that provides the most meaningful and complete information. When a report is prepared in more than one volume, repeat the primary title, add volume number, and include subtitle for the specific volume. On classified documents enter the title classification in parentheses.

**Block 5. Funding Numbers.** To include contract and grant numbers; may include program element number(s), project number(s), task number(s), and work unit number(s). Use the following labels:

C - Contract	PR - Project
G - Grant	TA - Task
PE - Program Element	WU - Work Unit Accession No.

**Block 6. Author(s).** Name(s) of person(s) responsible for writing the report, performing the research, or credited with the content of the report. If editor or compiler, this should follow the name(s).

**Block 7. Performing Organization Name(s) and Address(es).** Self-explanatory.

**Block 8. Performing Organization Report Number.** Enter the unique alphanumeric report number(s) assigned by the organization performing the report.

**Block 9. Sponsoring/Monitoring Agency Name(s) and Address(es).** Self-explanatory.

**Block 10. Sponsoring/Monitoring Agency Report Number.** (If known)

**Block 11. Supplementary Notes.** Enter information not included elsewhere such as: Prepared in cooperation with...; Trans. of...; To be published in.... When a report is revised, include a statement whether the new report supersedes or supplements the older report.

**Block 12a. Distribution/Availability Statement.** Denotes public availability or limitations. Cite any availability to the public. Enter additional limitations or special markings in all capitals (e.g. NOFORN, REL, ITAR).

**DOD** - See DoDD 5230.24, "Distribution Statements on Technical Documents."

**DOE** - See authorities.

**NASA** - See Handbook NHB 2200.2.

**NTIS** - Leave blank.

**Block 12b. Distribution Code.**

**DOD** - Leave blank.

**DOE** - Enter DOE distribution categories from the Standard Distribution for Unclassified Scientific and Technical Reports.

**NASA** - Leave blank.

**NTIS** - Leave blank.

**Block 13. Abstract.** Include a brief (*Maximum 200 words*) factual summary of the most significant information contained in the report.

**Block 14. Subject Terms.** Keywords or phrases identifying major subjects in the report.

**Block 15. Number of Pages.** Enter the total number of pages.

**Block 16. Price Code.** Enter appropriate price code (*NTIS only*).

**Blocks 17. - 19. Security Classifications.** Self-explanatory. Enter U.S. Security Classification in accordance with U.S. Security Regulations (i.e., UNCLASSIFIED). If form contains classified information, stamp classification on the top and bottom of the page.

**Block 20. Limitation of Abstract.** This block must be completed to assign a limitation to the abstract. Enter either UL (unlimited) or SAR (same as report). An entry in this block is necessary if the abstract is to be limited. If blank, the abstract is assumed to be unlimited.